Received: 2 August 2023 | Revised: 1 January 2024 | Accepted: 14 February 2024

DOI: 10.1002/eqe.4105

RESEARCH ARTICLE

WILEY

Simplified state-dependent seismic fragility assessment

Mabel Orlacchio[1,2] | **Georgios Baltzopoulos**[2] | **Iunio Iervolino**[2,3]

[1]Ministero delle Infrastrutture e dei Trasporti, Rome, Italy

[2]Dipartimento di Strutture per l'Ingegneria e l'Architettura, Università degli Studi di Napoli Federico II, Naples, Italy

[3]IUSS – Scuola Superiore Universitaria di Pavia, Pavia, Italy

Correspondence
Georgios Baltzopoulos, Dipartimento di Strutture per l'Ingegneria e l'Architettura, Università degli Studi di Napoli Federico II, Naples, Italy.
Email: georgios.baltzopoulos@unina.it

Funding information
Horizon 2020, Grant/Award Number: 821115; Ministero dell'Università e della Ricerca; RELUIS

Abstract

Earthquakes are clustered in time and space; therefore, structures may be subjected to multiple consecutive instances of potentially damaging shaking, with insufficient in-between time for repair operations to take place. Methodologies to evaluate the risk dynamics in this situation require vulnerability models that are able to capture the transitions between damage states, from the intact conditions to failure, due to multiple damaging earthquakes, that is, state-dependent fragility curves. One of the state-of-the-art methods for the assessment of structure-specific state-dependent fragility curves relies on a variant of *incremental dynamic analysis* (IDA), which is often termed *back-to-back* or B2B-IDA. The computational costs typically involved in B2B-IDA motivate attempts to simplify the evaluation of state-dependent fragility curves. This paper presents a simplified method for multi-story moment-resisting frame structures, based on pushover analysis in conjunction with a predictive model for the main features of a damaged structural system, such as residual deformations and loss of stiffness and/or strength. The predictive model enables the probabilistic definition of the post-earthquake pushover curve of a damaged structural system, given the displacement demand imposed by a preceding damaging shock. The state-dependent fragility curves are then evaluated via IDA of single-degree-of-freedom oscillators based on these pushover curves. Illustrative applications validate the ability of the proposed methodology to provide state-dependent fragilities with reduced computational costs compared to the back-to-back IDA method.

KEYWORDS
damage accumulation, pushover-based method, sequence-based seismic reliability

1 | INTRODUCTION

The usual practice of seismic risk assessment does not consider that structural failure can be reached progressively due to damage accumulation in multiple earthquakes. Moreover, it is generally assumed that a structure is initially in intact conditions. These assumptions can be justified by considering that, for example, after some seismic event damages the structure of interest, enough time will elapse until the next earthquake to repair it.[1] However, the nature of seismic events is such that they typically occur in time-space clusters, which means that the necessary repair time between shocks may not be available and that damage to buildings and infrastructure may accumulate rapidly.[1,2]

A practical quantitative model for structural vulnerability, in the context of seismic risk assessment, is represented by the fragility function that provides the conditional probability that the structure fails to meet some performance objective, given that a ground-shaking intensity measure (IM) has some specific value (im). This failure is often termed exceedance of a so-called *damage*-state (DS). Although seismic structural damage could be quantified by continuous measures, practical considerations typically dictate the definition of a finite number of DS. In the simplest of cases, damage states can be defined by means of an engineering demand parameter (EDP), and a series of threshold values, whose exceedance is taken to signify the transition of the structure from its initial state to another one representing worse conditions.

Certain risk assessment methods, able to model damage accumulation,[3,4] require a set of fragility curves for each structure. These curves provide the probability of the structure transitioning between any pair of damage states from intact conditions to failure; therefore, these curves are named state-dependent fragility functions. More specifically, state-dependent fragility can be defined as the conditional probability that, given the occurrence of any shaking intensity, a structure that was in a damage state DS_i, goes into a more severe damage state DS_j:

$$P\left[DS_j|DS_i \cap IM = im\right] = P\left[EDP > edp_{DS_j|DS_i}|DS_i \cap IM = im\right]. \quad (1)$$

For example, if one assumes four discrete damage states that a structure can be in, then $i = 0, 1, 2, 3$ and $j = 1, 2, 3, 4$ with $j > i$. In this context, DS_0 can be taken to mean the intact state, while the notation $edp_{DS_j|DS_i}$ signifies the response threshold that a structure in damage state i must cross to transition into damage state j.

State-of-the-art analytical derivation of classical structural fragility, $P[DS_j|DS_0 \cap IM = im]$, entails subjecting the numerical model of the structure to numerous nonlinear dynamic analyses, for example, via incremental dynamic analysis (IDA),[5,6] which consists in collecting the non-linear responses of an (initially undamaged) structure to a set of records, each one progressively scaled in amplitude to represent different levels of seismic intensity. For the evaluation of state-dependent fragility curves, an extended version of IDA has been suggested, referred to here as back-to-back or B2B-IDA.[7–14] According to this method, the structural model is first subjected to a set of records, representing a first seismic event hitting the structure at its intact state. Each record of the set is scaled in amplitude to the lowest value of IM that causes the structure to reach the damage state DS_i, $i = 1, 2, 3$. Thus, at the end of each record, a different realization of the damaged structural model is produced. Subsequently, each incarnation of the structural model in DS_i is subjected to another (or the same) set of accelerograms simulating an aftershock. Each record of the second set is scaled until the damaged structure reaches a more severe damage state, say DS_j, with $j > i$. The state-dependent fragility $P[DS_j|DS_i \cap IM = im]$ can then be derived by collecting the scaled intensities of all records in the second set, possibly fitting a parametric model based on those results, as will be discussed in more detail later on.

The derivation of fragility curves via IDA can be computationally demanding.[14–16] This has motivated the development of simplified procedures for analytical fragility development, based on static nonlinear analysis (*pushover analysis*). These methods consist in substituting the complex numerical model with an equivalent inelastic single-degree-of-freedom (SDoF) system, whose definition is based on the original structure's pushover curve. One such example, used in the case of traditional fragility assessment, is the method proposed by Vamvatsikos and Cornell,[17] which has been recently streamlined into a dedicated software tool.[18] Because the number of required dynamics analyses is increased by orders of magnitude in the case of B2B-IDA, the need of simplified procedures to derive state-dependent fragility is even greater.[19] This has motivated the study presented herein, where a pushover-based methodology is proposed for the assessment of state-dependent fragility curves for multi-story moment-resisting frame structures. While this method uses *equivalent* SDoF models to simplify the fragility assessment, it also seeks to further reduce the computational cost by eschewing the need for the first step dynamic analysis required to bring the structure to the damage state of interest, DS_i. Instead, instances of the damaged structural configuration are obtained via Monte-Carlo simulation. This simulation is based on a model that enables the generation of a series of realizations of the pushover backbones representing the structure's SdoF approximation when it is in the given damage state of interest. The development of this analytical model, which provides the joint probability distribution of residual displacement, stiffness deterioration and strength degradation for inelastic SDoF systems with evolutionary hysteresis, is also an integral part of the present study.

The presentation of this work is organized as follows: first, the development of the predictive model needed for the stochastic generation of backbone curves for the structure that is in a specific damage state is outlined. Subsequently, the model's application in a Monte-Carlo simulation context is presented. Then, the simplified methodology for state-dependent fragility derivation is presented, incorporating the aforementioned model. This method is further illustrated

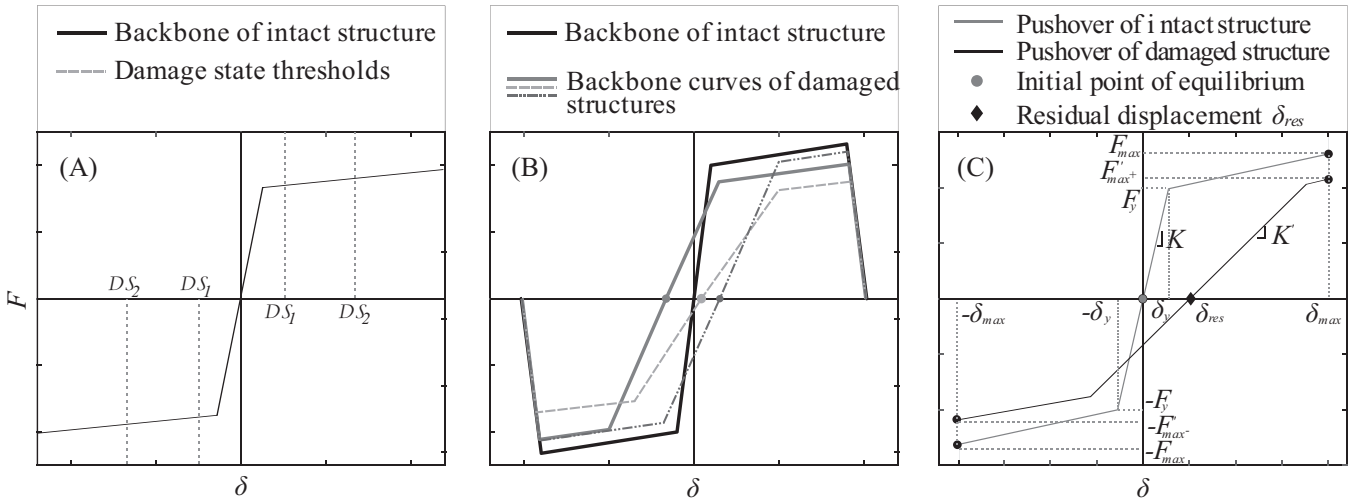

FIGURE 1 Definition of damage via deformation thresholds (A); post-shock backbones and residual displacements of an SDoF system evaluated for three different records scaled to cause the same damage state (B); examples of an SDoF structure's monotonic pushover (backbone) curve before and after the seismic damage for a generic stiffness- and strength-degrading system (C).

via an application, and the results are compared to those obtained via the rigorous procedure involving sequential dynamic analysis. Finally, some concluding remarks close the paper.

2 | SIMULATION OF THE STATIC PUSHOVER OF A DAMAGED STRUCTURE

The simplified method for state-dependent fragility assessment developed herein is based mainly on two simplifications. The first one consists in replacing the multi-degree-of-freedom structural model with a surrogate structure in the form of an equivalent inelastic single-degree-of-freedom (ESDoF) system, defined based on the original structure's pushover curve. The second simplification consists in generating a sample of SDoF models representing the structure in some damage state, without performing nonlinear dynamic analyses, but based on a predictive model instead. In this context, the transition of a structure from one damage state to another during an earthquake shock is defined based on crossing some threshold transient displacement, δ_{max}, (Figure 1A) as per common earthquake engineering practice.[20]

However, δ_{max} is a convenient but indirect measure of structural damage and there is no guarantee that if a specific structure is nominally brought to the same damage state by different base-acceleration time histories, other mechanical characteristics such as stiffness, strength and residual displacement will be the same. For example, one can take a SDoF inelastic structure whose response to cyclic loading is characterized by evolutionary hysteretic rules and whose backbone curve is shown in Figure 1B. This structure was subjected to three different accelerograms that all brought it at the same peak transient displacement and, consequently, the same damage state. The figure also shows the three pushover curves obtained after each of the accelerograms has nominally led the structure to the same *DS*. It can be observed that there is some variability in the reloading stiffness, maximum restoring force and residual displacement that each incarnation of the damaged structure exhibits and the present study seeks to capture that variability with an analytical model. As will be shown later, these structural properties exhibit similar record-to-record variability, for a given inelastic excursion, when it comes to multiple degree-of-freedom frame structures.

2.1 | Methodology

The first stepping-stone in the direction of simplified state-dependent fragility is the development of a semi-empirical model for the static pushover curve (or monotonic *backbone*) of a SDoF oscillator after it has been subjected to an earthquake shock that has resulted in a given displacement demand. This model was developed for simple inelastic systems that can be deemed to be representative of high- and low-code frame structures with flexure dominated inelastic response. These systems are yielding oscillators characterized by piece-wise linear backbone and peak-oriented hysteretic behaviour,

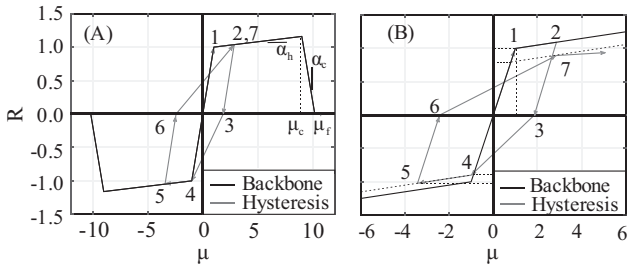

FIGURE 2 Peak-oriented modified IMK hysteretic model. Backbone curve and quasi-static cyclic response of an inelastic SDoF system without any cyclic strength degradation, shown in dimensionless $\{R, \mu\}$ coordinates (A); quasi-static cyclic response that includes cyclic strength degradation (B).

potentially exhibiting cyclic strength degradation. The analytical model adopted for the numerical implementation of the hysteretic rule was the modified *Ibarra-Medina-Krawinkler* (IMK) model.[21,22] An example trilinear backbone is shown in Figure 2A using dimensionless $\{R, \mu\}$ coordinates, where $R = F/F_y$ is the strength ratio of the elastic force over the yield base shear of the system, and $\mu = \delta/\delta_y$ stands for the response-to-yield displacement ratio, that is, the ductility.[2] The analyzed systems have backbone curves consisting of an elastic branch followed by a post-yield hardening segment, the latter defined by a hardening slope α_h and ending at a capping point ductility μ_c.

Among the various types of degradation contemplated by this hysteretic model, two types are considered in this study: (i) degradation of the reloading stiffness inherent in the peak-oriented model, where the direction of the loading path targets the maximum displacement on the opposite side, once the horizontal axis is intersected in each reloading cycle (e.g., Figure 2A); (ii) *cyclic* strength degradation, where the maximum attainable restoring force is reduced every half-cycle of response, by an amount proportional to the dissipated hysteretic energy.[23] Figure 2 displays the cyclic response of two of the simple inelastic systems considered here, behaving according to the modified IMK rule; the one in panel (A) corresponds to a case without cyclic strength degradation, whereas panel (B) shows a system that does exhibit cyclic strength deterioration. Note that cyclic strength degradation is so-termed to distinguish it from in-cycle degradation, the latter being a designation often used in the literature[24] to describe situations where ductility demand exceeds the capping point μ_c and strength is lost as the response follows down the softening branch of the monotonic backbone. It should be clear that no ductility demands $\mu > \mu_c$ are considered in this investigation, and therefore no in-cycle strength degradation ever comes into play in the development of the model; the descending softening branch, defined by a post-capping slope α_c and intercepting the zero-strength axis at a failure ductility, μ_f, is only shown for completeness.

The static pushover of the damaged structure shown in Figure 1B is defined by three parameters, that is, the residual displacement, δ_{res}, the post-shock reloading stiffness, K', and the post-shock lateral resistance, $F'_{max\pm}$. For the specific hysteretic rule considered here, if these three parameters are known, in addition to the initial backbone of the undamaged structure, it is possible to completely define the backbone curve of the damaged structure.[25] In fact, the method developed in this study revolves around a probabilistic description of the aforementioned main parameters that enable simulation: (i) the constant-ductility residual displacement ratio, C_μ, (ii) the relative period elongation, ΔT and (iii) the loss of lateral strength ΔR. C_μ is defined as:

$$C_\mu = \frac{\delta_{res}}{\delta_{max}}, \tag{2}$$

that is the ratio of the residual displacement, δ_{res}, and peak transient displacement, δ_{max}, both caused by the same base-acceleration.[26,27] ΔT is a measure of the loss of lateral stiffness of the structure during ground shaking and is defined as:

$$\Delta T = \frac{(T' - T)}{T}, \tag{3}$$

where T' is the post-shock period and T is the period of the SDoF structure in intact, pre-shock condition. The elongated period is calculated as $T' = 2 \cdot \pi \cdot \sqrt{m/K'}$, where K' was defined as the post-shock reloading stiffness as shown in Figure 1C. Finally, ΔR quantifies a normalized loss of lateral strength and is defined as:

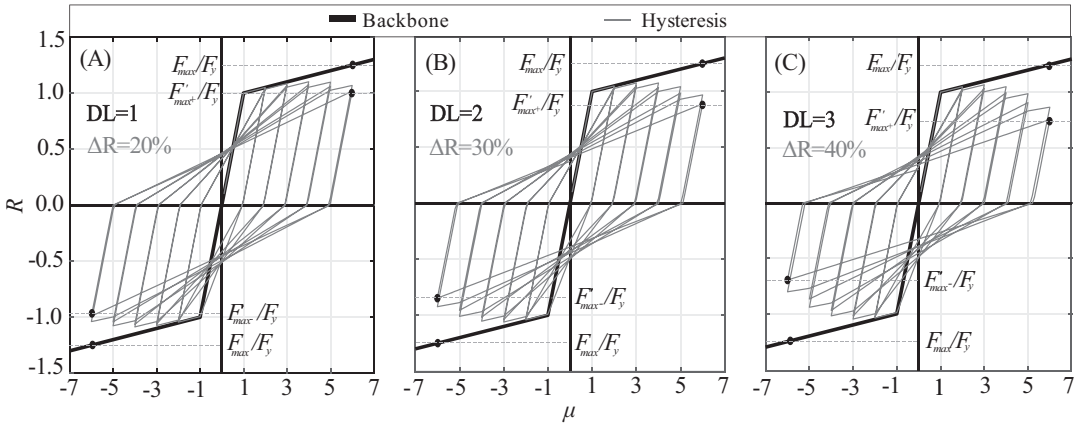

FIGURE 3 Three conventional levels of strength degradation used in this study, defined on the basis of strength loss after a quasi-static cyclic loading protocol: low-degradation peak-oriented hysteretic rule (A); medium-degradation (B); high-degradation (C).

$$\Delta R = 1 - \frac{F'_{max+} + |F'_{max-}|}{2 \cdot F_{max}}, \tag{4}$$

where $F_{\max} = F_y \cdot [1 + \alpha_h \cdot (\mu - 1)]$ is the maximum restoring force reached along the hardening branch of the initial backbone when pushed at ductility μ under static loading (i.e., in the absence of cyclic strength degradation), F_y and α_h are the yield force and hardening slope of the intact structure, respectively; $F'_{max\pm}$ is the maximum force in both the horizontal loading directions, that corresponds to the same ductility on the deteriorated backbone after the system has been subjected to cyclic loading; that is, on the pushover of the damaged structure, as shown in Figure 1C (the evaluation of F'_{max+} and F'_{max-} and is performed upon the backbones of the damaged structure that have been shifted from the initial point of equilibrium by the residual displacement δ_{res}). Hereafter, F'_{max} is used to express the deteriorated lateral resistance at maximum ductility demand, evaluated as $F'_{max} = 1/2 \cdot (F'_{max+} + |F'_{max-}|)$, which simplifies Equation (4) to $\Delta R = 1 - F'_{max}/F_{max}$. Because these parameters are affected by record-to-record variability, the model developed treats parameters C_μ, ΔT and ΔR as random variables (RVs). The objective of the model is to provide their conditional joint probability distribution, given the maximum transient ductility demand $\mu = \delta_{max}/\delta_y$ that has been induced by an earthquake shock to a series of SDoF oscillators. That joint distribution of the three RVs, in turn, enables the definition of a set of pushover curves representing multiple realizations of the corresponding structure at a damage state DS_i, that can be associated with ductility demand μ.

Overall, the SDoF systems considered for the development of the predictive model had eight different periods of natural vibration; that is, $T = \{0.3s, 0.6s, 0.9s, 1.0s, 1.2s, 1.5s, 1.8s, 2.0s\}$, eight distinct hardening stiffness ratios ranging from zero to ten percent of the elastic stiffness, $\alpha_h = \{0\%, 0.5\%, 1\%, 2\%, 3\%, 4\%, 5\%, 10\%\}$ and four levels of cyclic strength degradation. These cyclic strength degradation levels will be hereafter arbitrarily referred to as cases of low-, medium- and high-degradation, also including a non-degrading case. This conventional labelling of the three degradation levels was calibrated so that ΔR would result approximately equal to 0.20, 0.30 and 0.40 for the low-, medium- and high-degradation levels, respectively, at the end of a displacement-controlled quasi-static cyclic loading, as shown in Figure 3 (for more details on the degradation-controlling parameters of the modified IMK rule, the interested reader can consult the work of Lignos and co-authors).[22] The loading protocol used for this definition based on ΔR, which is used to quantify loss of strength as illustrated in the figure, consisted of performing two symmetric full cycles, gradually increasing ductility from $\mu = 2$ to 6 in five steps. For the sake of parsimony in notation, the index DL is hereafter used to distinguish the SDoF systems according to level of strength degradation, taking values of 0, 1, 2 and 3 in order to indicate: no degradation, low, medium and high levels of degradation, respectively.

The combination of all these variants led to a total of two-hundred and fifty-six inelastic SDoF systems used in the analyses that will be described in what follows. Each SDoF oscillator was modelled numerically using the OpenSees platform (*Open System for Earthquake Engineering Simulation*)[28] via the DYANAS software,[12] and subjected to a suite of one hundred single-horizontal-component earthquake ground motions, selected from the NESS dataset.[29] These records were recorded on firm soil at a closest-to-rupture-plane distance ranging from 0 to 44.5 km and were produced by earthquakes with moment magnitude belonging to the 6.1–7.6 range. The records are devoid of apparent pulse-like directivity effects and exhibit peak ground acceleration ranging from 0.05 to 1.40 g. Each accelerogram was iteratively scaled

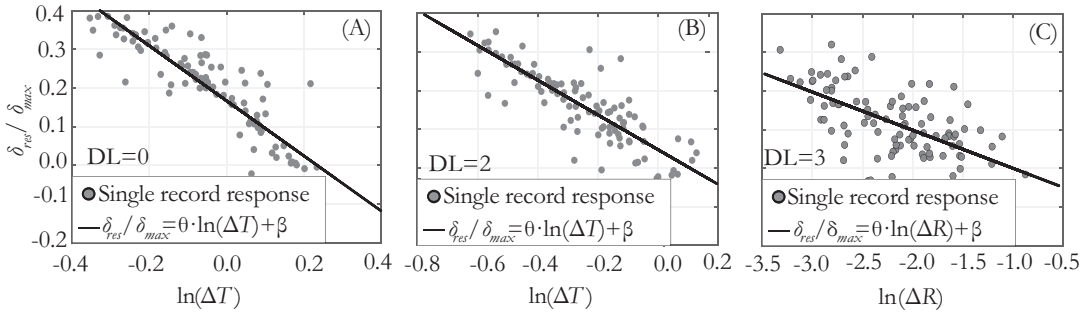

FIGURE 4 Examples of regression of $\delta_{res}/\delta_{max}$ against $\ln(\Delta T)$ and against $\ln(\Delta R)$, highlighting their (negative) linear correlation. Shown here are the cases of an SDoF system with $\alpha_h = 1\%, T = 1.0s$ and $\mu = 5$ without strength deterioration (A); $\alpha_h = 5\%, T = 1.2s$ and $\mu = 4$ with a medium level of strength deterioration (B); $\alpha_h = 10\%, T = 1.2s$ and $\mu = 4$ with a high level of strength deterioration (C).

via IDA[5] to result in nine levels of ductility demand for each SDoF structure, specifically $\mu = \{1.5, 2, 3, 4, 5, 6, 7, 8, 9\}$. It is recalled that all these ductility values end-up on the hardening branch of the oscillators' backbones, with no in-cycle degradation being involved in the inelastic excursions. The viscous damping ratio of all SDoF models was set at $\xi = 5\%$.

At the end of each dynamic analysis, during which the SDoF systems reach fixed ductility levels, whose attainment can be regarded as defining a damage level for the structure, the residual displacement δ_{res} is recorded and a static pushover analysis is performed, in both positive and negative loading directions. Zero-padding the end of the acceleration record provides the time needed for damping-out any remaining velocity of the mass, prior to the measurement of δ_{res} and onset of the pushover. Therefore, for each SDoF system and fixed ductility demand, one-hundred manifestations of the damaged structure's static pushover curve are obtained, from which the degraded reloading stiffness K' and deteriorated lateral resistance at maximum ductility demand F'_{max} can be measured, along with δ_{res}. These analytical results are subsequently used for the development of the model.

2.2 | Model for residual displacement

The analyses described in the preceding section provided samples of residual displacement δ_{res}, remaining at the end of a seismic excitation causing given displacement demand δ_{max}. This is accompanied by the post-event backbone of the SDoF system, which means that the corresponding stiffness- and possible strength-degradation can be quantified. This data is used to derive a model for $C_\mu = \delta_{res}/\delta_{max}$.

The natural logarithm of the relative increase in period $\ln(\Delta T)$, already defined in Equation (3), is the chosen measure of stiffness degradation. Strength degradation is quantified via $\ln(\Delta R)$, with ΔR given by Equation (4). Note that the few cases exhibiting $\Delta R > 0.50$, that is, loss of lateral resistance exceeding fifty percent of the initial, were held to represent situations of incipient collapse and were not given further consideration.

The starting point for defining the model is the relation that was observed between the ratio of residual to peak transient displacement C_μ and $\ln(\Delta T)$, for the simplest case where strength degradation is absent. It was observed[30] that C_μ exhibits persistently negative correlation with $\ln(\Delta T)$, for varying T, μ and α_h, that is, the correlation coefficient,[31] $\rho_{\ln(\Delta T),C_\mu}$, between these two quantities ranges from -0.50 to -0.99 with $|\rho_{\ln(\Delta T),C_\mu}| \geq 0.7$ for the majority of cases examined, with the few exceptions corresponding to cases of ductility demand of $\mu \geq 7.0$, and some of the longer periods of natural vibration considered; that is, $T \geq 1.8s$. This is illustrated in Figure 4A, where one-hundred $\delta_{res}/\delta_{max}$ responses against the corresponding $\ln(\Delta T)$ values are plotted, along with the regression line of the former versus the latter.

Both δ_{res} and δ_{max} preserve their sign in this formulation, so that the ratio becomes negative when the two occur in opposite directions. Furthermore, the same level of negative correlation between C_μ and $\ln(\Delta T)$ also persists in the case of SDoF systems exhibiting cyclic strength deterioration, which can be seen in the second panel of the figure. For example, the cases shown in the first two panels of Figure 4 are characterized by $\rho_{\ln(\Delta T),C_\mu}$ equal to -0.93 and -0.88, respectively.

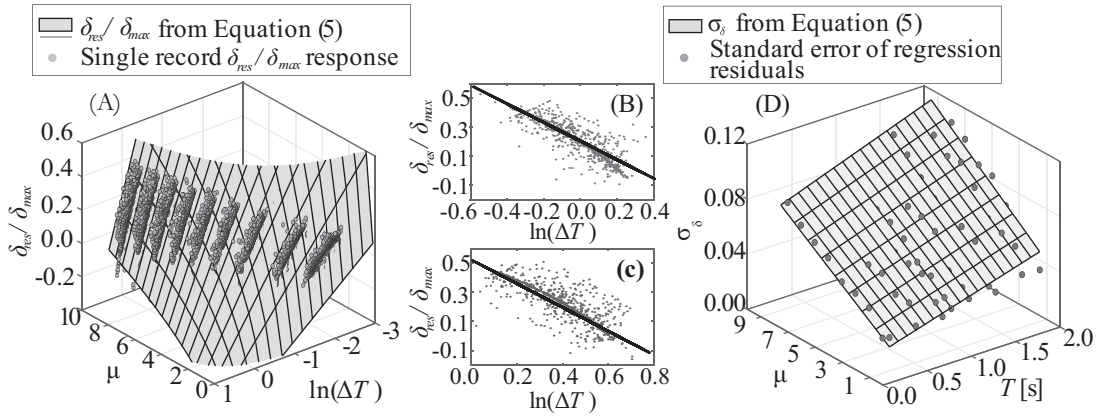

FIGURE 5 Central tendency and standard deviation of the model for the residual displacements in case of absent strength deterioration. Central tendency for $\alpha_h = 0$ and multiple ductility demands (A); central tendency for $\alpha_h = 0$ and $\mu = 5$ (B); central tendency for $\alpha_h = 0$ and $\mu = 8$ (C); standard deviation σ_δ for $\alpha_h = 3\%$ (D).

In cases with cyclic strength degradation, a negative correlation was also observed between C_μ and $\ln(\Delta R)$, across all T, μ and α_h considered (see Figure 4C), with correlation coefficients ranging from −0.3 to −0.8, and with $|\rho_{\ln(\Delta R),C_\mu}| \geq 0.5$ for the majority of analyzed cases. Based on this observed trend, a linear model was adopted for the expected value of C_μ in case of no strength degradation ($DL = 0$). In this case, the slope and intercept of the model are only functions of the ductility demand μ and of the post-yield hardening ratio α_h. Thus, the model for C_μ without strength degradation is:

$$\begin{cases} C_\mu = \theta_1 \cdot \ln(\Delta T) + \beta_1 + \varepsilon_0 \cdot \sigma_\delta \\ \theta_1 = b_{C1} + b_{C2} \cdot \sqrt{\mu - 1} + b_{C3} \cdot \alpha_h \\ \beta_1 = c_{C1} + c_{C2} \cdot \sqrt{\mu - 1} + c_{C3} \cdot \alpha_h \cdot \sqrt{\mu - 1} \\ \sigma_\delta = d_{C1} \cdot T + d_{C2} \cdot (\mu - 1) + d_{C3} \cdot \alpha_h + d_{C4} \cdot \alpha_h \cdot (\mu - 1) + d_{C5} \cdot (\mu - 1) \cdot T \cdot \alpha_h \end{cases} \quad (5)$$

where ε_0 is a standard Normal random variable, θ_1 and β_1 represent the slope and intercept of the model and σ_δ is the standard deviation of the regression residuals. θ_1 and β_1 are modelled as functions of μ and α_h. The model parameters, b_{C_k} and c_{C_k} with $k = 1, 2, 3$, were estimated by means of *robust regression*[31] of C_μ against $\{\ln(\Delta T), \mu, \alpha_h\}$ using iteratively re-weighted least squares with bisquare weighting. The analytical form of the model for θ_1 and β_1 was determined by performing preliminary linear regressions against the analysis results, separately for the various SDoF systems and ductility levels considered (e.g., Figure 4) and observing the variation of these two parameters with respect to μ, α_h and ΔT graphically. The heterogeneity of data around the mean, expressed via the standard deviation of the logs σ_δ, was found to be non-constant, varying with the model covariates, and was thus modelled using least-squares curve-fitting of the analytical expression in Equation (5).

Figure 5 shows a plot of the models for $\delta_{res}/\delta_{max}$ and standard deviation σ_δ in case of $DL = 0$. Panel (A) refers to the case of $\alpha_h = 0$ and for the cases with $\mu = 5$ and $\mu = 8$ in panels (B) and (C), respectively, whereas the remaining plot shows the model of standard deviation σ_δ in the case of $\alpha_h = 3\%$.

The model for C_μ in case of $DL = 1, 2, 3$ was defined as:

$$\begin{cases} C_\mu = \theta_1 \cdot \ln(\Delta R) + \beta_1 + \gamma_1 \cdot \ln(\Delta R)^{-2} + \varepsilon_0 \cdot \sigma_\delta \\ \theta_1 = b_{C1} + b_{C2} \cdot \sqrt{\mu - 1} + b_{C3} \cdot \alpha_h \\ \beta_1 = c_{C1} + c_{C2} \cdot \sqrt{\mu - 1} + c_{C3} \cdot \alpha_h \cdot \sqrt{\mu - 1} \\ \sigma_\delta = d_{C1} \cdot T + d_{C2} \cdot (\mu - 1) + d_{C3} \cdot \alpha_h + d_{C4} \cdot (\mu - 1)^2 \end{cases} \quad (6)$$

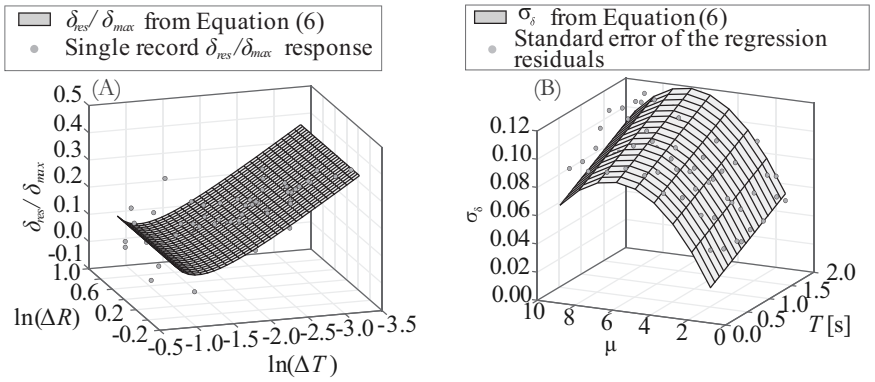

FIGURE 6 Central tendency and standard deviation of the model for the residual displacements in case of medium strength deterioration. Central tendency for $\alpha_h = 1\%, \mu = 6$ and $T = 0.6s$ (A); standard deviation σ_δ in the case of $\alpha_h = 1\%$ (B).

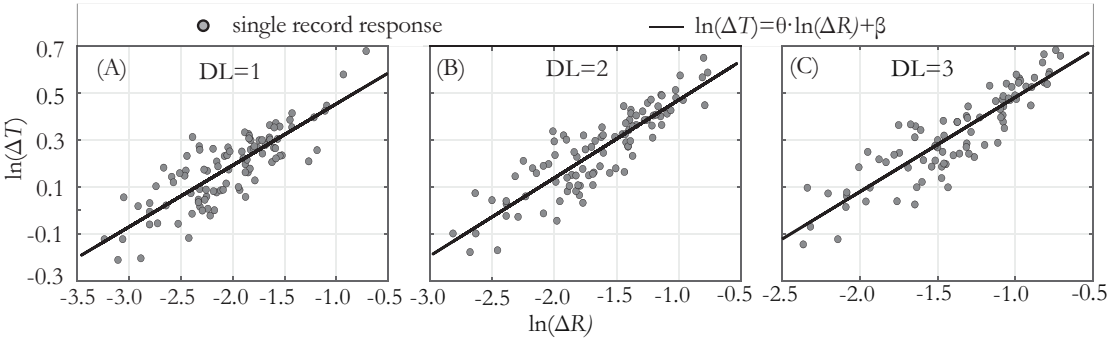

FIGURE 7 Examples of correlation between $\ln(\Delta T)$ and $\ln(\Delta R)$ for an SDoF system with $\alpha_h = 5\%, T = 0.3s$ and $\mu = 6$ in case of low level of strength deterioration (A); medium level of strength deterioration (B) and high level of strength deterioration (C).

The model of the expected value of C_μ in case of $DL = 1, 2, 3$ is a function of the variable $\ln(\Delta R)$ and includes a non-linear term, that is $\ln(\Delta R)^{-2}$. Also in this case, θ_1 and β_1 are expressed as linear combinations of various simple functions of μ and α_h. The parameters b_{C_k} and c_{C_k} with $k = 1, 2, 3$ and model parameter γ_1 are again estimated using robust regression, applied for each DL separately. Standard deviation σ_δ was found to be non-constant in these cases as well, and was modelled, by means of least-squares curve-fitting, as shown in Equation (6). The figure below shows an example of the $\delta_{res}/\delta_{max}$ from the model (Figure 6A) and σ_δ (Figure 6B) for a system with $\alpha_h = 1\%, \mu = 6$ and $T = 0.6s$, considering $DL = 2$.

The alternative use of the predictor variables $\ln(\Delta T)$ and $\ln(\Delta R)$ in the regression model of Equations (5) and (6) can be justified by the correlation between these two random variables observed for all DL and T, μ, α_h ranges considered, as shown in Figure 7. Completeness of the model required the definition of the joint distributions of C_μ, $\ln(\Delta R)$ and $\ln(\Delta T)$ in case of strength degradation, or that of C_μ and $\ln(\Delta T)$ in the case where strength degradation is absent. To this end, the relationship between $\ln(\Delta T)$ and $\ln(\Delta R)$ was examined and Mardia's test[32] was performed with the null hypothesis being that the two are jointly Normal distributed, for given initial characteristics of the structure T , α_h, DL and for a fixed ductility demand μ. The results showed that in almost all cases the null hypothesis could not be rejected at a 5% significance level. Based on this result, it was assumed that $\{\ln(\Delta T), \ln(\Delta R)\}$ is a bivariate Gaussian random vector, whose joint distribution can be completely defined knowing the marginal distributions of $\ln(\Delta T)$ and $\ln(\Delta R)$, and their correlation coefficient, $\rho_{\ln(\Delta T),\ln(\Delta R)}$.

2.3 | Model for period elongation

The model for period elongation was first developed for the case of no strength degradation, $DL = 0$, with subsequent modifications introduced for the three levels $DL = 1, 2, 3$. The marginal distribution of period elongation was defined assuming a Lognormal model for ΔT. The functional form adopted for the expected value of ΔT stems from observing trends of ΔT data against the inelastic portion of the ductility demand, $(\mu - 1)$, for each pair of T and α_h. Fitting of the model's parameters to the data was performed via weighted least squares regression because of the non-constant variance

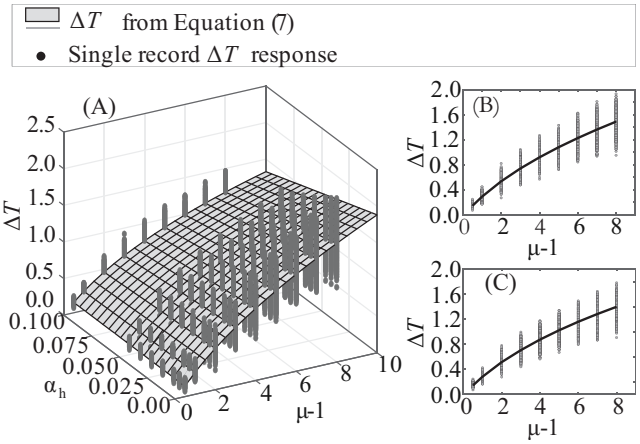

FIGURE 8 Model for period elongation in case of no strength degradation. Model for the central tendency of period elongation (A); median period elongation for $\alpha_h = 0.03$ (B) and for $\alpha_h = 0.05$ (C).

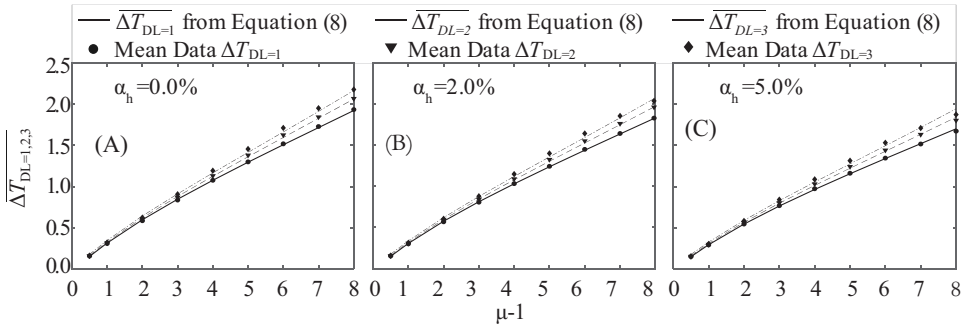

FIGURE 9 Increments in terms of ΔT for the three levels $DL = 1, 2, 3$ in case of $\alpha_h = 0$ (A); $\alpha_h = 2\%$ (B) and $\alpha_h = 5\%$ (C).

and the analytical form of the model in case of $DL = 0$ is reported in Equation (7):

$$\begin{cases} \overline{\Delta T} = b_{T1} + b_{T2} \cdot \alpha_h \cdot \mu^{-1/2} + b_{T3} \cdot \alpha_h \cdot \mu + b_{T4} \cdot \mu^{1/2} \\ \sigma_{\Delta T} = d_{T1} + d_{T2} \cdot \overline{\Delta T} \end{cases} \tag{7}$$

where $\overline{\Delta T}$ is the mean of the Lognormal model with standard deviation $\sigma_{\Delta T}$, which is estimated as the standard error of the regression residuals. The terms $b_{T\mathrm{k}}$ with $k = 1, .., 4$ are the model parameters.

An analytical expression was also proposed for expressing $\sigma_{\Delta T}$ as a function only of $\overline{\Delta T}$. The parameters $d_{T\,k}$, $k = 1, 2$, appearing in Equation (7) are estimated from curve-fitting against the regression residuals for the level of strength degradation $DL = 0$. Figure 8 shows a graph of the model, highlighting the dependence of its central tendency on α_h and μ, with panels (b) and (c) showing the expected value for period elongation in absence of strength degradation for the cases of $\alpha_h = 0.03$ and $\alpha_h = 0.05$.

It was observed that the ΔT data for $DL = 1, 2, 3$ followed a trend similar to $DL = 0$, with somewhat larger values, on average. For this reason, this part of the model was developed by processing the data of each degradation level separately and modelling the differences obtained between the data and the expected value of ΔT from Equation (7). In the end, the period elongation mean, $\overline{\Delta T_{DL\,=\,1,2,3}}$, was evaluated by adding to $\overline{\Delta T}$ another two terms with some dependence on μ, as shown in Equation (8):

$$\begin{cases} \overline{\Delta T_{DL=1,2,3}} = \overline{\Delta T} + b_{T5} + b_{T6} \cdot \mu^2 \\ \sigma_{\Delta T, DL=1,2,3} = d_{T1} + d_{T2} \cdot \overline{\Delta T_{DL\,=\,1,2,3}} \end{cases}. \tag{8}$$

In the cases of $DL = 1, 2, 3$, the standard deviation of period elongation, $\sigma_{\Delta T, DL\,=\,1,2,3}$ was also modelled as a function of the mean, $\overline{\Delta T_{DL\,=\,1,2,3}}$. The parameters b_{T5}, b_{T6}, d_{T1}, d_{T2}, were calibrated for each level of strength degradation. Figure 9

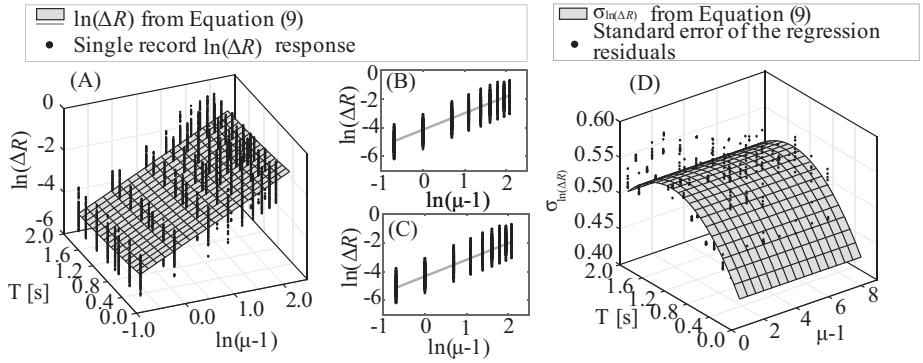

FIGURE 10 Model for strength loss for the case of low-level strength degradation. Model for mean $\ln(\Delta R)$ in case of $\alpha_h = 0.01$ (A); central tendency of strength reduction in case of $\alpha_h = 0.01$ and $T = 0.6\ s$ (B); central tendency of strength reduction in case of $\alpha_h = 0.01$ and $T = 1.5\ s$ (C); model of standard deviation $\sigma_{\ln(\Delta R)}$ (D).

shows the ΔT increments for the three levels of strength degradation in cases of $\alpha_h = 0$, $\alpha_h = 2\%$ and $\alpha_h = 5\%$.

2.4 | Model for strength loss

The model for strength loss provides the ΔR parameter of the post-shock structure at a fixed ductility demand μ, given the initial characteristics of the structure T , α_h and DL. The data showed a linear trend of ΔR with $(\mu - 1)$, in log-space, for each pair of T and α_h and for each level of strength degradation. The proposed model is:

$$\begin{cases} \ln\ (\Delta R) = \theta_3\ \cdot \ln(\mu - 1) + \beta_3 + \varepsilon_2 \\ \theta_3 = b_{R1}\ + b_{R2} \cdot \alpha_h \\ \beta_3 = c_{R1}\ + c_{R2} \cdot \alpha_h + c_{R3} \cdot T + c_{R4} \cdot T^2 \\ \sigma_{\ln(\Delta R)} = d_{R1}\ + d_{R2} \cdot T + d_{R3} \cdot T^2 + d_{R4} \cdot (\mu - 1) + d_{R5} \cdot (\mu - 1)^2 \end{cases} . \tag{9}$$

The central trend of $\ln(\Delta R)$ was found to exhibit some dependence on the initial period of natural vibration, T, and on the post-yield hardening ratio α_h. In Equation (9), the parameters b_{Rk} with $k = 1, 2$ and c_{Rk} with $k = 1, .., 4$, were evaluated by curve fitting of the results performed for each level of strength degradation using a weighted least squares regression because of the non-constant variance. The term ε_2 is a zero mean Gaussian variable with standard deviation $\sigma_{\ln(\Delta R)}$, which was estimated as the standard error of the regression residual and was found to be dependent on the period of the intact structure and the ductility demand, as reported in Equation (9). The parameters d_{Rk}, $k = 1, 2, .., 5$ appearing in Equation (9), were estimated from curve-fitting against the regression residuals. Examples of the models for the mean and standard deviation of $\ln(\Delta R)$ are reported in Figure 10. The first panel of the figure shows the model for the mean of $\ln(\Delta R)$ for a system with hardening slope $\alpha_h = 0.01$ and low strength deterioration level, while the last panel shows the model of $\sigma_{\ln(\Delta R)}$ for the same level of degradation.

To define the joint distribution of $\ln(\Delta T)$ and $\ln(\Delta R)$, the definition of the covariance matrix Σ of the bivariate Gaussian vector $\{\ln(\Delta T), \ln(\Delta R)\}$ is needed:

$$\Sigma = \begin{bmatrix} \sigma^2_{\ln(\Delta T)} & \sigma_{\ln(\Delta T)} \cdot \sigma_{\ln(\Delta R)} \cdot \rho_{\ln(\Delta T),\ln(\Delta R)} \\ \sigma_{\ln(\Delta T)} \cdot \sigma_{\ln(\Delta R)} \cdot \rho_{\ln(\Delta T),\ln(\Delta R)} & \sigma^2_{\ln(\Delta R)} \end{bmatrix} . \tag{10}$$

The covariance matrix is defined by the (estimated) standard deviations of the logarithms of period elongation $\sigma_{\ln(\Delta T)}$ and strength loss $\sigma_{\ln(\Delta R)}$ and their (estimated) correlation, $\rho_{\ln(\Delta T),\ln(\Delta R)}$, with the standard deviations being obtainable from Equations (8) and (9) . The correlation coefficient $\rho_{\ln(\Delta T),\ln(\Delta R)}$ was modelled as a linear function of the ductility demand and hardening slope until a transition ductility μ_t is reached:

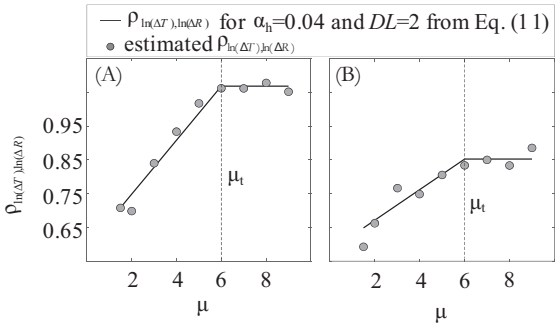

FIGURE 11 Model for $\rho_{\ln(\Delta T),\ln(\Delta R)}$ in case of medium strength degradation and $\alpha_h = 0.04$ for $T < 1.5$ s (A) and $T \geq 1.5$ s (B).

$$\rho_{\ln(\Delta T),\ln(\Delta R)} = e_1 + e_2 \cdot (\mu - 1) + e_3 \cdot \alpha_h \quad 1.5 \leq \mu \leq \mu_t. \tag{11}$$

In case of $\mu > \mu_t$, $\rho_{\ln(\Delta T),\ln(\Delta R)}$ varies only as function of α_h and can be evaluated from Equation (11) assuming $\mu = \mu_t$. The value of μ_t differs by level of strength degradation, that is, it is assumed equal to 7 for $DL = 1$; 6 for $DL = 2$ and 5 for $DL = 3$ based on data observation. The coefficients e_k, $k = 1, 2, 3$ in Equation (11) were defined by curve-fitting of the results performed separately for each level of strength degradation. Moreover, it was necessary to distinguish the fitting procedure of the model parameters into two separate cases $T < 1.5$s and $T \geq 1.5$s. Figure 11 shows the model of $\rho_{\ln(\Delta T),\ln(\Delta R)}$ evaluated for the medium strength degradation and $\alpha_h = 0.04$ for the case of $T < 1.5$s and $T \geq 1.5$s.

All the coefficients in the equations from Equations (5) to (11) are reported in tabular form in Orlacchio (2022)[33] and also as an electronic supplement to the present paper (see Data availability section).

2.5 | Model implementation and validation

Once the models for period elongation, strength deterioration and residual displacement have been completely specified, it is possible to determine the joint distribution of $\{\ln(\Delta T), \ln(\Delta R), C_\mu\}$, given the ductility demand μ, period T, hardening slope α_h and the level of strength degradation DL. The implementation discussed herein relies on Monte Carlo simulation, the first step of which entails selecting fixed values of μ, T, α_h, and DL, and then calculating $\overline{\ln(\Delta R)}$, and $\sigma_{\ln(\Delta R)}$ via Equation (9). Then, a realization of $\ln(\Delta R) = x_i$ is extracted from a normal distribution having these parameters (here i subscript indicates that the context is that of the i-th out of N programmed simulations). At this point, it is possible to define the distribution of $\ln(\Delta T)$ conditional on $\ln(\Delta R) = x_i$ as:

$$\begin{cases} \mathrm{E}\left[\ln(\Delta T) \,|\ln(\Delta R) = x_i\right] = \overline{\ln(\Delta T)} + \rho_{\ln(\Delta T),\ln(\Delta R)} \cdot \left(\sigma_{\ln(\Delta T)}/\sigma_{\ln(\Delta R)}\right) \cdot \left[x_i - \overline{\ln(\Delta R)}\right] \\ \sigma_{\ln(\Delta T)|\ln(\Delta R)} = \sqrt{\left(1 - \rho^2_{\ln(\Delta T),\ln(\Delta R)}\right) \cdot \sigma^2_{\ln(\Delta T)}} \end{cases}, \tag{12}$$

where $\mathrm{E}[\ln(\Delta T)|\ln(\Delta R) = x_i]$ represents the conditional mean of $\ln(\Delta T)$ and $\sigma_{\ln(\Delta T)|\ln(\Delta R)}$ the conditional standard deviation. Both Normal distribution parameters $\overline{\ln(\Delta T)}$ and $\sigma_{\ln(\Delta T)}$ are calculated from Equation (8) using known transformations from the lognormal model parameters $\overline{\Delta T}$ and $\sigma_{\Delta T}$. Then, a value of $\ln(\Delta T) = y_i$ is sampled from the Normal distribution whose parameters are given by Equation (12). Finally, the conditional mean and standard deviation of the ratio C_μ is evaluated from Equation (6) given the sampled vector of $\{x_i, y_i\}$ and the i-th random sample of $C_{\mu,i} = z_i$ is extracted from the corresponding Normal distribution. (In the case of no strength degradation, the Monte-Carlo scheme degenerates into sampling a value $\ln(\Delta T) = y_i$, from the marginal distribution of $\ln(\Delta T)$, and then directly sampling $\delta_{res}/\delta_{max} = z_i$ from its conditional distribution.)

By repeating the sampling procedure an arbitrary number of times, say N, one can obtain a representation of the joint densities of these RVs in the form of relative frequency diagrams of the sampled values. An example of such a representation is reported in Figure 12, which was constructed using one million samples. A feature that is worth commenting is the slight distortion exhibited by the simulated joint distribution of period elongation and residual displacement ratio, shown in Figure 12B, towards the region of higher $\ln(\Delta T)$ values. This can be attributed to the contribution of the non-

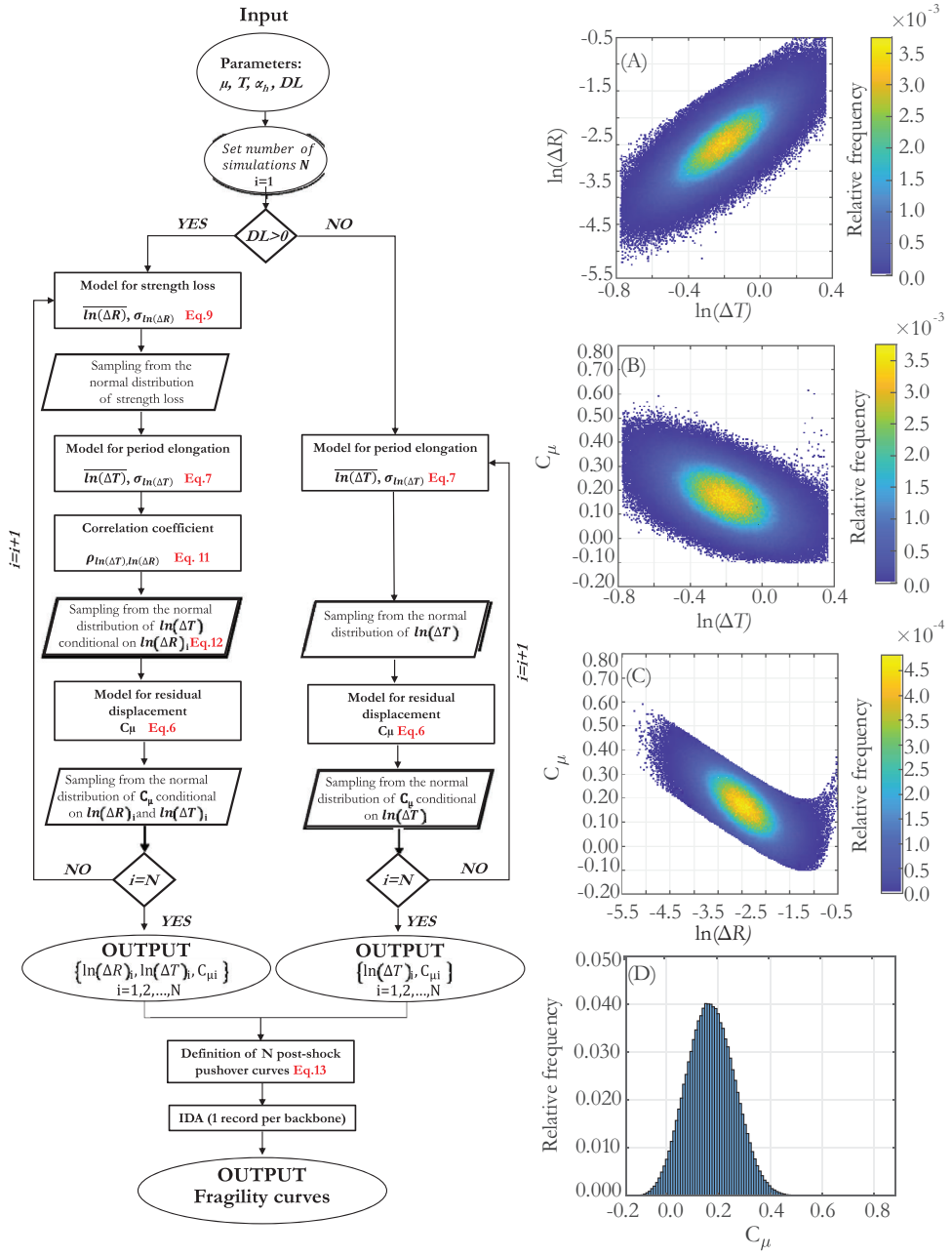

FIGURE 12 Monte-Carlo-based representation (relative frequency) of the joint distribution of period elongation and strength reduction (A), of period elongation and residual displacement (B), of strength reduction and residual displacement (C), for the case of ductility demand $\mu = 4$, post-yield hardening ratio $\alpha_h = 3\%$, period of the initial structure $T = 0.8\ s$ and medium level of strength degradation; Monte Carlo based representation of the marginal distribution of C_μ (D); flowchart of the simulation procedure in the context of the proposed methodology for state-dependente fragiltity assessment on the left side.

linear terms involving $\ln(\Delta R)$ in Equation (9). For the same reason, there is a similar effect visible in the shape of the joint density of C_μ and $\ln(\Delta R)$ in panel c.

Each sample of the random vector $\{\ln(\Delta T), \ln(\Delta R), C_\mu\}$ obtained according to the procedure described enables to univocally define the corresponding bilinear backbone curve of the SDoF oscillator at the end of a seismic excitation causing a given ductility demand. In other words, the Monte-Carlo simulation provides realizations of the post-shock pushover curve of the SDoF system, representing a relation of the damaged state of the considered system, as illustrated in Figure 13. This figure shows the coordinates of the points defining the initial and post-shock curve in the displacement-force plane, using the notation with primes for the parameters of the damaged system. The elastic branch of the damaged system's pushover can be determined by evaluating the yield force $F'_{y\pm}$ and displacement $\delta'_{y\pm}$ in the positive and negative direc-

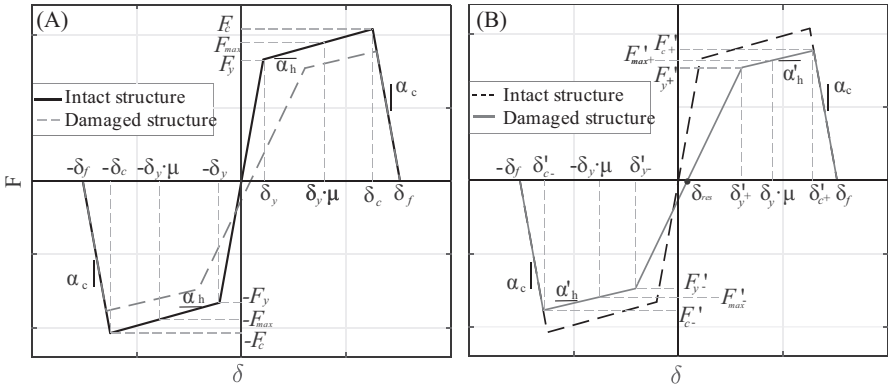

FIGURE 13 Parameters defining the pushover curves; parameters for the definition of the intact structure's pushover curve (A); and of the post-shock pushover curve (B).

tions, whereas the post-yield branch is defined by the hardening slope α'_h, the capping point displacements in the two directions, $\delta'_{c\pm}$ and corresponding forces $F'_{c\pm}$. The relations allowing to assess the parameters defining the post-shock curve as function of the parameters defining the pushover curve of the initial structure and the ductility demand are:

$$\begin{cases} F'_{y\pm} = \left[F'_{\max} - F'_{\max} \cdot \frac{\alpha_h}{\delta_y} \cdot \frac{F_y}{F_{\max}} \cdot \left(\mu \cdot \delta_y \mp \delta_{res}\right)\right] \Big/ \left[1 - \frac{F'_{\max}}{F_{\max}} \cdot \alpha_h \cdot \left(\frac{T'}{T}\right)^2\right] \\ \delta'_{y\pm} = \delta_y \cdot \frac{F'_{y\pm}}{F_y} \cdot \left(\frac{T'}{T}\right)^2 \pm \delta_{res},\ \alpha'_h = \alpha_h \cdot \frac{F'_{\max}}{F_{\max}} \cdot \left(\frac{F_y}{F'_{y\pm}} \cdot \frac{\delta'_{y\pm} \mp \delta_{res}}{\delta_y}\right) \end{cases} . \tag{13}$$

It is worth recalling that the model was developed considering only ductility demands that maintain structural response displacement along the hardening branch, without crossing into any potential softening branch where in-cycle strength degradation would occur. In the example shown in the figure, the capping point and softening branch are included solely for illustrative purposes, under the arbitrary assumption that the post-cap slope α_c and rupture displacement δ_f would remain invariant during the system's transition from intact to damaged.

A twofold validation of the predictive model was undertaken. First, the distributions of C_μ resulting from the model via the Monte-Carlo resampling scheme were compared with the data used for the development of the model for various SDoF systems and ductility demands. Subsequently, for a single case, the damaged structure pushovers predicted by the model were compared to dynamic and static non-linear analysis results of multiple-degree of freedom (MDoF) systems. For the first case, the validation was made by calculating the 25th, 50th and the 75th percentiles of residual displacement ratio for each combination of μ, α_h, T and DL and comparing the results from the resampling procedure with the corresponding percentiles estimated from the initial data set. For the sake of brevity, two comparisons are reported here as examples, showing general agreement of the distribution percentiles obtained from the model with those of the data set used in the regressions. Figure 14 shows the results obtained for the case of no strength degradation ($DL = 0$) and $\alpha_h = 0.01$ considering μ between 1.5 and 9.0 and four natural vibration periods T (i.e. 0.3, 0.9, 1.2, 1.8 s). Figure 15 shows the results obtained for the case of high strength degradation ($DL = 3$) and $\alpha_h = 0.02$ for all the values of μ from 1.5 to 9.0 and the same four T as the previous figure (i.e. 0.3, 0.9; 1.2; 1.8 s). In both the figures, the results obtained from the model are represented using black lines (dashed lines for 25th and 75th percentiles and solid line for the 50th percentile). On the other hand, the reference data are reported using a box plot representation in which the central mark indicates the median, and the top and the bottom edges of the box indicate the 25th and 75th percentiles, respectively.

For the second instance of model validation, three moment-resisting frames (MRFs) were used: a reinforced concrete (RC) four-story MRF without masonry infills and two steel perimeter MRFs. All are fixed-base plane models, with the RC MRF shown in Figure 16A. A lumped plasticity approach was adopted for modelling nonlinear structural behavior, using multi-linear moment-plastic rotation relations and the modified IMK model without cyclic strength degradation for the definition of the hysteretic behaviour. The RC MRF has a first-mode period of natural vibration equal to 0.53 and exhibits first-mode dominated dynamic elastic response with a participating mass ratio at the first mode close to 90%. Capacity design against shear means that inelastic response of the constituent beams and columns is flexure-dominated.

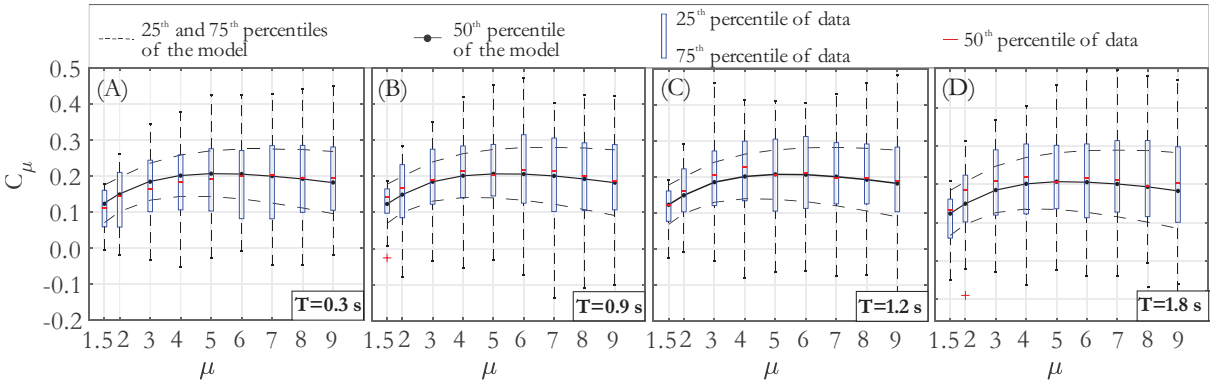

FIGURE 14 Comparison of the summary statistics in case of no strength degradation and $\alpha_h = 0.01\%$ for periods equal to 0.3 s (A); 0.9 s (B); 1.2 s (C); and 1.8 s (D).

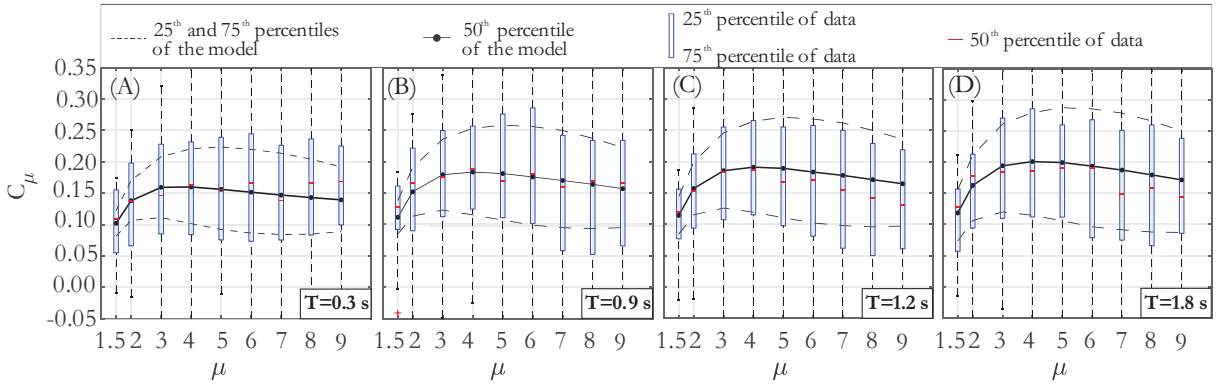

FIGURE 15 Comparison of the summary statistics in case of high level of strength degradation and $\alpha_h = 0.02\%$ for periods equal to 0.3 s (A); 0.9 s (B); 1.2s (C); and 1.8 s (D).

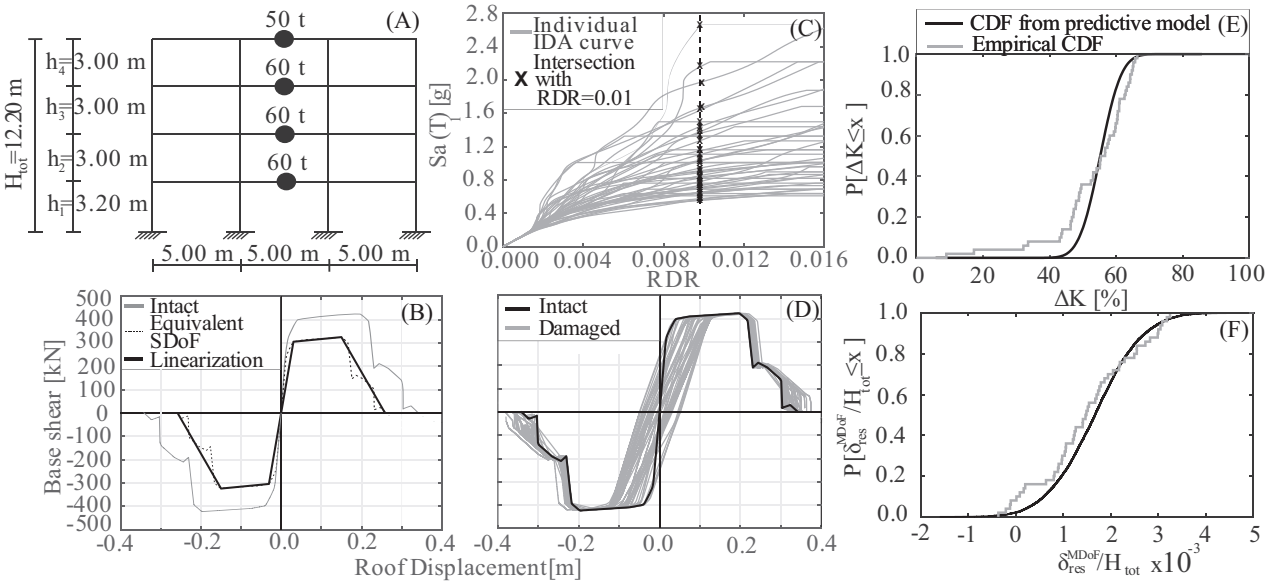

FIGURE 16 Comparison of model predictions with dynamic analysis results of the RC MRF: characteristics of the example four-story frame (A); pushover of the frame and equivalent SDoF backbone (B); IDA curves of the MDoF structure (C); pushover curves for the damaged frame after each record (D); comparison of predicted and empirical distributions of the stiffness reduction (E) and residual roof drift ratio (F).

TABLE 1 Mean and standard deviation defining the distributions of the period elongation and of the constant-ductility residual displacement ratio.

Structure		$\overline{\ln(\Delta T)}$	$\sigma_{\ln(\Delta T)}$	$\overline{C_\mu}$	σ_δ
Four-storey RC MRF	Predictive model	0.494	0.168	0.223	0.112
	MDoF results	0.467	0.153	0.209	0.127
Two-storey steel MRF	Predictive model	0.215	0.048	0.130	0.075
	MDoF results	0.208	0.061	0.159	0.095
Four-storey steel MRF	Predictive model	0.458	0.075	0.163	0.080
	MDoF results	0.475	0.113	0.218	0.140

The two steel MRFs, a two- and a four-storey frame with first-mode periods of 0.94 and 1.21 s, respectively, are part of a series of steel buildings designed for the purposes of a past study,[34] where more detailed information on geometry and dynamic properties can be found. Of these frames, the response of the four-storey steel MRF is the most sensitive to higher-mode effects, having a first-mode participating mass ratio near 80% and influence of higher-mode effects documented in past work.[18] For the purposes of this validation, equivalent SDoF systems were defined, based on static nonlinear analyses that were carried out by applying a gradually increasing lateral force profile corresponding to each structure's first-mode excitation to base acceleration, shown for the RC frame in Figure 16B. The predictive model was applied for the equivalent SDoF systems representative of the intact structure. The backbone of each equivalent SDoF oscillator was obtained by dividing each frame's pushover force and roof displacement values by the first-mode participation factor, Γ, and obtaining a multi-linear approximation of the resulting curve. In the multi-linear approximation for the RC MRF shown in the figure, $\Gamma = 1.309$ and the nominal yield point of the equivalent SDoF system is taken to correspond to a roof drift ratio (RDR) of 0.0033, that is, the point of formation of a global plastic mechanism for the structure, while its mass m^*, period T^* and hardening slope α_h are 147 t, 0.77s and 0.017, respectively. It is arbitrarily assumed that entry of the frame into a generic damage state occurs when the RDR exceeds a threshold value of 0.01. The MDoF system was subjected to incremental dynamic analysis using as input a set of fifty acceleration records, none of which were included in the suite of records employed for the development of the model. For the execution of the IDA, the pseudo-acceleration at the fundamental period of vibration, $Sa(T_1)$, was assumed as intensity measure. Similar to the methodology used to develop the predictive model and presented in the previous paragraphs, the IDA results were used to determine the scale factor needed for each record to bring the structure at assumed damage state threshold, that is, a RDR of 0.01 (Figure 16C). Subsequently, the records thus scaled were used for the execution of dynamic analyses that were immediately followed by static non-linear analyses, again mimicking the previously described analysis methodology, resulting in different realizations of the damaged structure's pushover to be obtained, as shown in Figure 16D. On the other hand, the damage state threshold assumed for the two steel MRFs was a RDR of 0.02.

From these analyses, the residual roof displacements of the frame structures, δ_{res}^{MDoF}, were collected, along with the pushovers of the damaged systems, which were then approximated via piece-wise linear functions, for the sake of comparison with the results deriving from the application of the model. The mean and the standard deviation defining the distribution of the period elongation $\ln(\Delta T)$, from Equation (7) and the mean and standard deviation of the constant-ductility residual displacement ratio C_μ, obtained by means of Equation (5) and the Monte-Carlo simulation procedure, were compared with the estimates obtained from the analysis results of the MDoF model and are reported in Table 1.

The cumulative distribution functions of percentile loss of stiffness, ΔK, and residual RDR, $\delta_{res}^{MDoF}/H_{tot}$, obtained by means of the model and empirically using the RC frame's analyses results are compared in Figure 16E, F. In the figure, x represents a generic realization of the random variables ΔK and $\delta_{res}^{MDoF}/H_{tot}$, while the percentile loss of stiffness is computed as $\Delta K = |(K' - K)/K| = |(T/T')^2 - 1|$. The same results for the two steel frames are shown in Figure 17. It emerges that, for these case-study structures, the model was able to predict the statistics of the parameters defining the loss of stiffness of the damaged frame structures. While the same can be said about the residual displacements of the RC and two-storey steel MRFs, the results show somewhat larger values of mean and dispersion for the MDoF model of the four-storey steel MRF, with respect to the equivalent SDoF predictions. This can be attributed to the larger influence of higher modes to this frame's seismic response, alluded to previously, suggesting that provisions for MDoF effects should be taken in applications (to follow).

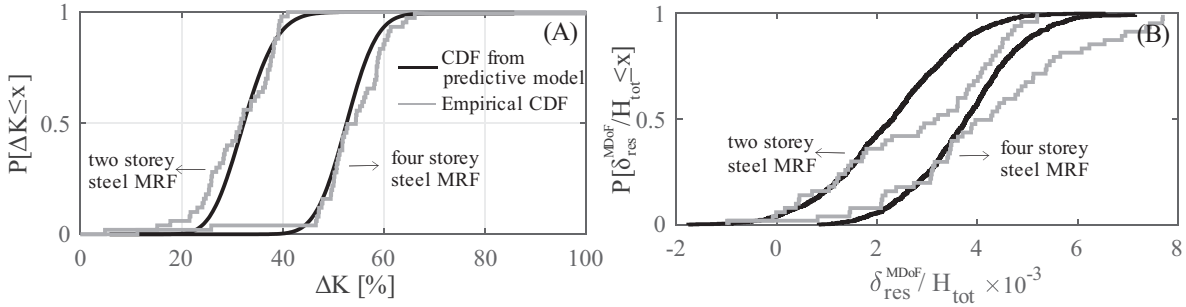

FIGURE 17 Comparison of model predictions with dynamic analysis results of two steel MRFs: comparison of predicted and empirical distributions of the stiffness reduction (A) and residual roof drift ratio (B).

3 | STATE-DEPENDENT SEISMIC STRUCTURAL FRAGILITY

The proposed simplified procedure for deriving sets of state-dependent fragility curves, consists of obtaining an equivalent SDoF system for the structure of interest, as described directly above, and then applying a parsimonious version of back-to-back IDA to that simpler inelastic system. In the original back-to-back IDA, each IDA curve is the product of two consecutively applied acceleration records: one scaled so as to bring the structure to the damage state DS_i and another scaled to increasing levels (im) of the ground-shaking intensity measure until the structural response reaches the $edp_{DS_j|DS_i}$ threshold which signals the transition from damage state DS_i to DS_j, $j > i$. Generally speaking, the shaking intensity that will bring the structure to DS_i is not known beforehand, so a full IDA needs to be run before the back-to-back analysis can start.

According to the procedure developed herein, the first part of back-to-back IDA can be replaced by generating a set of backbone curves for an equivalent SDoF system, via the model presented. As discussed, these backbones represent realizations of the damaged structure that has transitioned to DS_i due to a previous shock within an earthquake cluster. The second phase of the procedure consists of subjecting each damaged SDoF realization to a single-record IDA, similar to the analysis strategy used in an analogous context.[35] The result of this procedure is a set of IDA curves that can be used to evaluate the state-dependent fragilities. As with traditional IDA curves, the assessment of the state-dependent fragility function can be conducted using the IM-based approach, which introduces the RV of shaking intensity causing transition from damage state DS_i to DS_j, or $IM_{DS_j|DS_i}$. Therefore, a lognormal state-dependent fragility can be defined as:

$$\begin{cases} P\left[EDP > edp_{DS_j|DS_i}|DS_i \cap IM = im\right] = P\left[IM_{DS_j|DS_i} < im\right] = \Phi\left[\left(\ln(im) - \eta\right)/\beta\right] \\ \eta = ln\left(IM^{50\%}_{DS_j|DS_i}\right), \beta = 0.5 \cdot ln\left(IM^{84\%}_{DS_j|DS_i}/IM^{16\%}_{DS_j|DS_i}\right) \end{cases} \tag{14}$$

where η and β are the parameters (median and logarithmic standard deviation) of the lognormal model for $IM_{DS_j|DS_i}$, and where $\Phi(\cdot)$ is the standard Gaussian (cumulative) function. According to the equation, these fragility parameters η , β are estimated based on the median and 84%,16% fractiles, respectively denoted as $IM^{50\%}_{DS_j|DS_i}$, $IM^{84\%}_{DS_j|DS_i}$ and $IM^{16\%}_{DS_j|DS_i}$, obtained from analysis. More specifically, in the context of a complete back-to-back IDA analysis, these are the fractile values from a sample of n IDA curves, as shown in Figure 18, where $im_{DS_{j,k}}$ is the realization of the RV coming from the k-th two-record sequence, $k = 1, .., n$. In other words, $IM_{DS_j|DS_i} = im_{DS_{j,k}}$ is the shaking intensity of the second shock that causes $EDP = edp_{DS_j|DS_i}$, after a previous shock has caused $EDP = edp_{DS_j|DS_0}$.

In the context of the simplified procedure proposed here, $im_{DS_{j,k}}$ would represent a realization of the same RV but coming from a single accelerogram acting on an SDoF system with backbone curve obtained from the k-th Monte-Carlo simulation, according to the simulation procedure described earlier.

Note that, for the applications shown herein, all IDA curves use as intensity measure the spectral pseudo-acceleration at the period on the intact structure, $Sa(T)$, and an EDP that involves the maximum transient displacement, δ_{max}. However, several studies have observed that maximum transient displacement alone may not be able to adequately capture cumulative damage effects from multiple shocks.[3,36] Case-in-point, it was shown in the previous paragraphs that, for a given displacement demand, other structural parameters that can be said to be related to the degree of damage of a

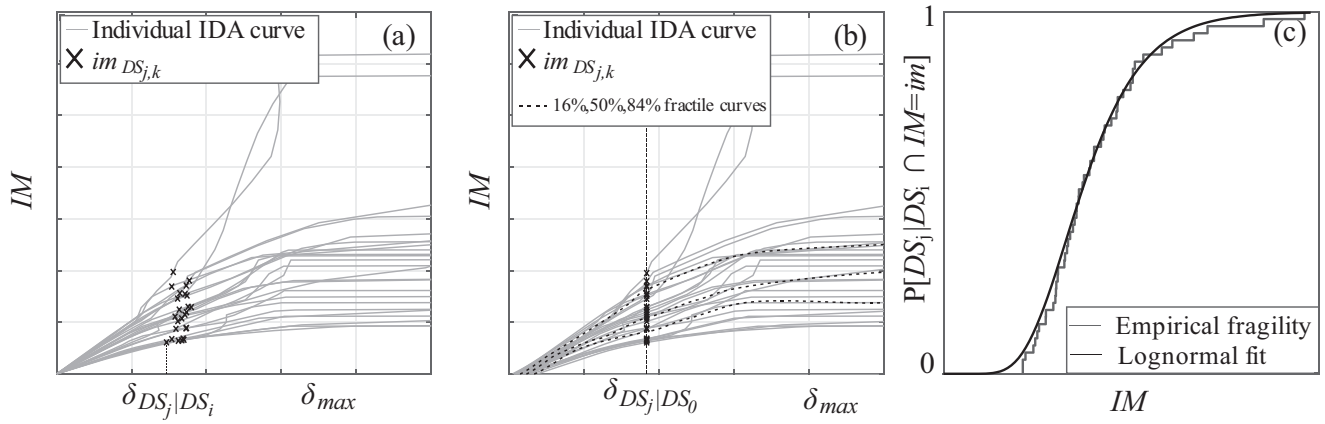

FIGURE 18 Example of (back-to-back) IDA curves and intensities causing damage state transition: transition EDP thresholds dependent on residual displacements (A); translated IDA curves to align transition intensities (B); state-dependent fragility assessment via the IM-based approach (C).

structure, such as the amount of stiffness or maximum restoring force lost, exhibit variability. It has also been suggested that, due to this variability, displacement-based thresholds may have to be adjusted for the purposes of state-dependent fragility definition,[37] or more elaborate *EDPs* should be used instead.[38] In this study, the amount of residual displacement is also involved in the damage measure for state-dependent fragility assessment, by assuming that the transition thresholds from damage state DS_i to DS_j can be obtained as:

$$\delta_{DS_j|DS_i} = \delta_{DS_j|DS_0} - \left|\delta_{res,DS_i}\right| \tag{15}$$

where $\delta_{DS_j|DS_0}$ is the displacement threshold defining the transition into the damage state DS_j when the structure starts from intact conditions and δ_{res,DS_i} is the residual displacement characterizing each realization of the damaged structure at DS_i. Under this assumption, each record's $im_{DS_{j,k}}$ value would correspond to a different realization of maximum displacement, as shown in Figure 18A. An alternative representation, more familiar to traditional IDA-based fragility assessment, is to shift each back-to-back IDA curve to the right by an amount equal to its first shock's residual $|\delta_{res,DS_i}|$, as shown in the second panel of the figure, so that the $im_{DS_{j,k}}$ values can be obtained from the intersection of each IDA curve with the vertical line passing from $\delta_{DS_j|DS_0}$. The last panel of the figure provides an example state-dependent fragility curve for the transition from DS_i to DS_j that would have resulted from these IDA curves in accordance with Equation (14).

In the following, the simplified procedure for state-dependent seismic fragility assessment is showcased through an illustrative application. It should be noted that the specific choice of *EDP* for the illustrative example, does not itself constitute a limitation for the procedure or an inextricable part thereof; since the procedure is based on analytical simulation of the damaged structure's backbone curve, any other *EDP* can be used, that is based on the information conserved in that simplified representation of the structure. Nevertheless, there are natural limitations for the applicability of the proposed procedure, that stem directly from the preceding discussion. First, applicability clearly hinges on the validity of associating a ductility (transient inelastic displacement) demand to a damage-state of the structure. This assumption is widely used for ductile frames, where capacity design principles allow most of the structural elements to develop plastic deformations and mobilize their inherent ductility in a uniform manner across the height, so that global measures of inelastic deformation such as RDRs can be held to be representative of the level of damage at a local level. In fact, recent studies have shown that using the simplification of a single *EDP* threshold to signify transition of such a structure from one *DS* to another, produces almost identical seismic reliability results as when the damage level of every single structural or non-structural element is monitored at every step of dynamic analysis to determine said transition.[20] Second, there are the relatively well-documented limitations dictated by the applicability of pushover-based procedures in general,[39] that is for the validity of using a surrogate SDoF inelastic oscillator to represent the displacement demand of the MDoF structure. These limitations include regularity in plan to avoid coupling of response in the two principal directions due to torsion, exclusion of high-rise frames due to influence of higher modes that cannot be captured by a surrogate SDoF system and seismic response characterized by evenly-distributed damage from plastic deformation across a multitude of structural

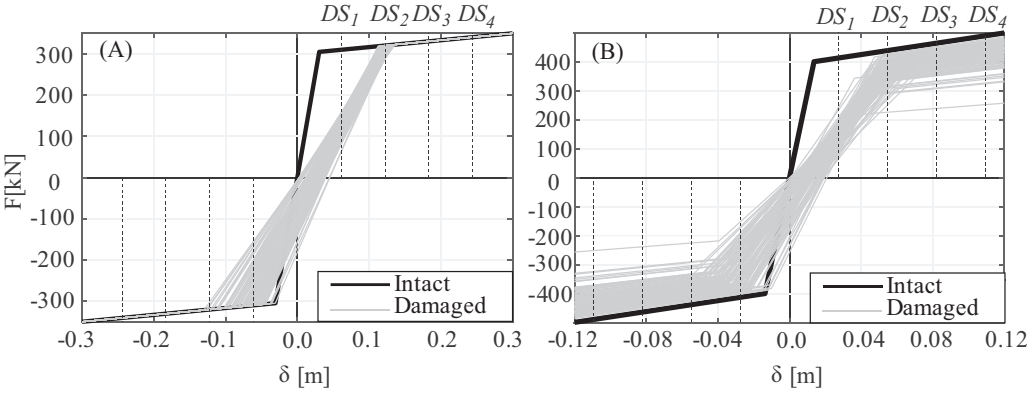

FIGURE 19 Backbone curve and definition of the damage states of the system 1 (A), backbone curve and definition of the damage states of the system 2 (B).

TABLE 2 Characteristics of the SDoF systems.

Systems	$T\,[s]$	$F_y\,[kN]$	$\delta_y\,[\mathrm{m}]$	α_h
1	0.77	304.81	0.0306	0.017
2	0.45	400.00	0.0137	0.032

TABLE 3 Damage states considered for the assessment of state-dependent fragility curves.

	Damage state	DS_1	DS_2	DS_3	DS_4
Systems	μ	2	4	6	8
1	$\delta_{DS_j\|DS_0}[\mathrm{m}]$	0.061	0.122	0.184	0.244
2	$\delta_{DS_j\|DS_0}[\mathrm{m}]$	0.027	0.055	0.082	0.110

elements, rather than localized damage possibly giving rise to brittle failure modes, with this last one being a requirement also shared by the first limitation above. Recent studies have shown that, in cases where these prerequisites hold, surrogate SDoF-based estimates of seismic reliability are in good agreement with those stemming from more elaborate numerical models.[40]

3.1 | Illustrative application

The objective of the application is to introduce in more detail the simplified method for state-dependent fragility assessment, and also to evaluate it, by comparing its results with fragility curves obtained using back-to-back IDA. For the application, two SDoF systems are considered as representative of moment-resisting RC frame structures. Although in pushover-based based methods the SDoF system is a proxy for the actual structure, which introduces additional sources of approximation, these examples consider directly SDoF systems, so as to isolate the consequences of the developed procedure from effects stemming from the multi- to single-DoF substitution. The periods of the two systems are $T = 0.77s$ and $T = 0.45s$, the hysteresis is assumed non-degrading for the first system and with the high level of strength degradation for the second one in order to test the effectiveness of the procedure in both cases. The bilinear backbone curves defining the SDoFs are shown in Figure 19 and their defining parameters are reported in Table 2.

To showcase the procedure, four damage states are arbitrarily defined, denoted from DS_1 to DS_4. The transition of the intact structures to the damage state DS_1 is considered to occur when the structural response of each system exceeds the threshold $\delta_{DS_1|DS_0}$ defined by a seismic ductility demand, μ, equal to 2, which corresponds to $\delta_{max} = 0.061\ m$ for the first system and to $\delta_{max} = 0.027\ m$ for the second one. In the same way, it is considered that the *direct* transition of the intact structure into DS_2, DS_3 and DS_4 (i.e. when the transition from intact to each DS_j is due to a single earthquake shock) occurs when μ exceeds the value of 4, 6 and 8, respectively, as reported in Table 3. The four damage state thresholds for each system, are also shown in Figure 19.

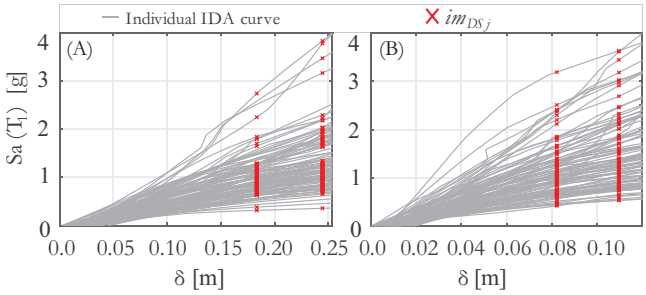

FIGURE 20 IDA curves obtained from the application of the simplified methodology for the first SDoF in case of DL = 0 and conditioning ductility equal to 4(A); for the second SDoF in case of DL = 3 and conditioning ductility equal to 4 (B).

TABLE 4 Median, e^{η}, and logarithmic standard deviation, β, defining the fragility curves for the two intact structures.

System	Cyclic degradation	Median e^{η} (g)				Standard deviation β			
		DS_1	DS_2	DS_3	DS_4	DS_1	DS_2	DS_3	DS_4
1	None	0.475	0.788	1.063	1.309	0.220	0.329	0.405	0.431
2	High	0.570	0.973	1.241	1.521	0.191	0.326	0.399	0.449

The threshold values $\delta_{DS_j|DS_0}$, used for the transition of the intact systems into one of the four generic damage states DS_j due to a single earthquake shock, are also considered in the definition of the thresholds defining the transition of the already-damaged system, according to Equation (15).

For each value of ductility demand considered, one-hundred backbone curves are generated according to the Monte Carlo procedure described. The backbones represent one hundred possible realizations of the pushover of the structure that has reached one of the four damages state corresponding to the ductility values. As an example, the backbone curves obtained considering $\mu = 4$ are given in Figure 19. (Note that in absence of strength degradation, see Figure 19A, the backbone curves of the damaged structure differ among themselves only in residual displacement and elastic stiffness.) Subsequently, for each set of one-hundred backbone curves each realization of the damaged system is subjected to IDA, using one record per extracted pushover, which is scaled upwards until the transition from the initial damage state (DS_1 , DS_2 or DS_3) to a more severe one occurs, that is, up to DS_4. These analyses were also run using the OPENSees finite-element platform, where a custom-made version of the modified IMK hysteretic model was implemented, which also allows for user-defined unloading stiffness. The IDA curves obtained in this manner are shown in Figure 20 for the two systems and for $\mu = 4$ where the im_{DS_j} points, obtained from their intersection with the vertical lines passing through $\delta_{DS_j|DS_0}$, are shown as red crosses. At this point, these im_{DS_j} values of each DS can be used to estimate the parameters of a lognormal model for the state-dependent fragility curves according to Equation (14). The IDA curves and all the results reported to follow are obtained using the pseudo-acceleration at the fundamental period of vibration of the intact structure, $S_a(T_1)$, as intensity measure.

To obtain a reference for comparing the results of this procedure, the same state-dependent fragilities were developed using back-to-back IDA, using a set of 20 records to represent the first damaging shock of the cluster, scaled to cause a ductility demand of two, four or six, and another 20 subsequent-shock accelerograms per initial shock, for a total of four-hundred curves (there was no overlap between the two sets of twenty records, but the same second-shock set was always paired to each first-shock record). Additionally, a 20-record IDA was used to estimate the intact structure's traditional fragility curves for the four damage states reported in Figure 19, that is, $P[DS_j|DS_0 \cap Sa\,(T_1) = sa]$. These runs were performed using an OPENSees user interface developed to streamline the back-to-back IDA.[12] The resulting median and standard deviations defining the fragility curves of the intact structures are reported in Table 4. The corresponding cumulative probability functions for the two SDoF systems are shown in Figure 21. Tables 5 and 6 collect the values of the median, η, and logarithmic standard deviation, β, defining the parametric state-dependent fragility curves for the two systems evaluated by means of the simplified procedure and of B2B-IDA procedure, respectively. In the tables, the third column gives the starting (conditioning) damage state DS_i, whereas the subsequent comluns report the fragility parameter per final damage state. The corresponding cumulative probability functions evaluated with the simplified procedure and the rigorous method of back-to-back IDA are shown in Figure 22 for the first system and in Figure 23 for the second one. Each figure shows the comparison between the state-dependent fragility curves evaluated using the simplified method

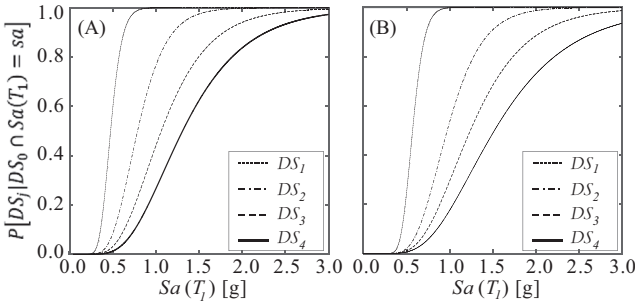

FIGURE 21 Fragility curves of intact structure evaluated considering four damage states using IDA for the SDoF system 1 (A) for the SDoF system 2 (B).

TABLE 5 Median, η, and logarithmic standard deviation, β, defining the state-dependent fragility curves of the two SDoF systems evaluated using the simplified methodology (e^{η} in g).

System	Cyclic strength degradation	DS_i	DS_2		DS_3		DS_4	
			e^{η}	β	e^{η}	β	e^{η}	β
1	none	DS_1	0.716	0.322	1.009	0.362	1.265	0.374
		DS_2	\	\	0.971	0.405	1.264	0.431
		DS_3	\	\	\	\	1.037	0.414
2	high	DS_1	0.885	0.391	1.228	0.423	1.538	0.451
		DS_2	\	\	1.049	0.450	1.329	0.470
		DS_3	\	\	\	\	1.218	0.501

TABLE 6 Median, η, and logarithmic standard deviation, β, defining the state-dependent fragility curves of the two SDoF systems evaluated using back-to-back IDA (e^{η} in g).

System	Cyclic strength degradation	DS_i	DS_2		DS_3		DS_4	
			e^{η}	β	e^{η}	β	e^{η}	β
1	None	DS_1	0.738	0.327	1.030	0.392	1.287	0.424
		DS_2	\	\	0.953	0.400	1.264	0.437
		DS_3	\	\	\	\	1.090	0.469
2	High	DS_1	0.888	0.336	1.183	0.404	1.474	0.448
		DS_2	\	\	1.095	0.422	1.410	0.462
		DS_3	\	\	\	\	1.253	0.490

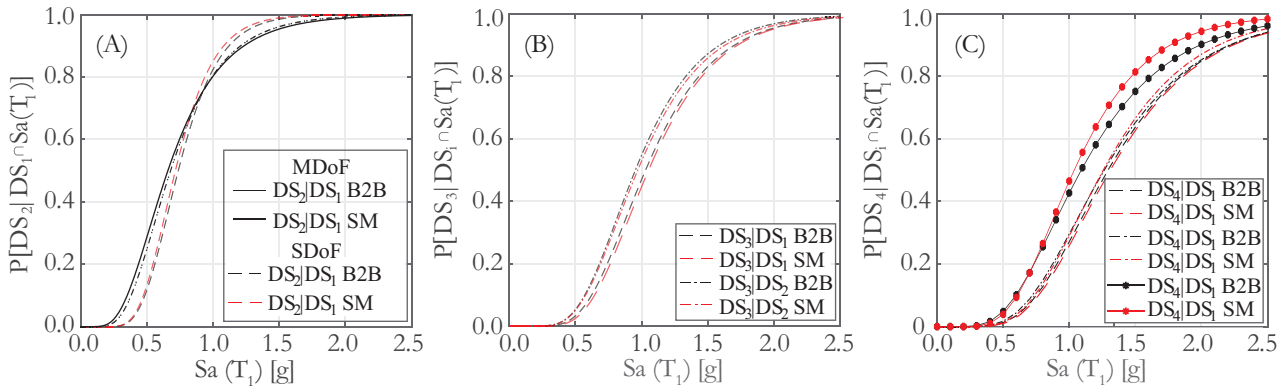

FIGURE 22 State-dependent fragility curves evaluated with the simplified methodology and the back-to-back IDA approach for the first case-study system.

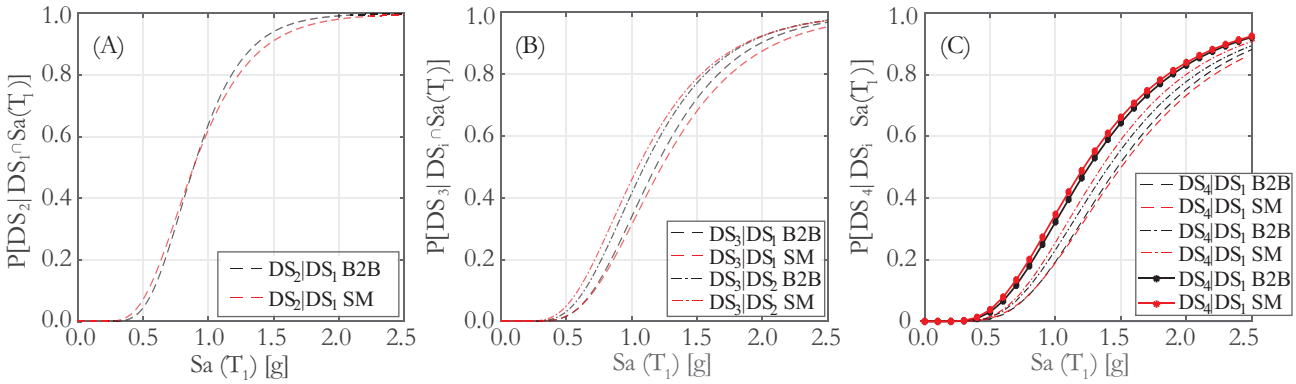

FIGURE 23 State-dependent fragility curves evaluated with the simplified methodology and the back-to-back IDA approach for the second case-study system.

'SM' and those deriving by back-to-back IDA *'B2B'*. Panels (A) of Figures 22 and 23 refer to transitions having DS_2 as the final damage state, whereas panel (B) and (C) refer to the final damage states DS_3 and DS_4, respectively.

Additionally, given that the first SDoF system shares the dynamic characteristics (Table 2) and initial hardening slope as the equivalent SDoF of the frame structure shown in Figure 16, and that the threshold for DS_2 shown in Figure 19 is prior to the capping point of the latter's pushover, it is possible to compare the state-dependent fragility $P[DS_2|DS_1 \cap IM = im]$ resulting from the simplified procedure with its counterpart obtained from B2B-IDA of the MDoF frame. As discussed earlier, application of the predictive model for MDoF systems may need to account for higher-mode effects influencing response in the non-linear range. Thus, for this comparison, the IDA curves from the simplified method are modified to account for higher-mode effects on the median and dispersion according to the methodology of the SPO2FRAG algorithm, which tends to correspond to a larger participating mass along the first mode when higher mode influence is of concern (more details can be found in Baltzopoulos and co-authors).[18] Another aspect of this comparison is an assessment of the savings in computational cost achieved by implementing the simplified procedure to derive the state-dependent fragility curves. This assessment can be performed at two levels, the first one being to compare the computing times required for implementation of the simplified procedure, versus the time required for running back-to-back IDA on a complete MDoF model. While it is intuitive to assume that this should depend on the complexity of the MDoF numerical model (e.g. by the number of structural elements involved), for the application presented here, the time required for the simplified procedure was about one-tenth of the time needed for the rigorous analysis of the MDoF system. The second level is to compare the time required for backbone simulation and dynamic analysis, compared to a full back-to-back IDA of the same equivalent SDoF system. Although, for this second case, the time saving varies from one acceleration record to another, an average of 30% reduction of computational time was calculated from the applications conducted herein, attributable to the substitution of some of the needed runs with Monte-Carlo simulations using the analytical model.

4 | FINAL REMARKS

The objective of the study presented in this paper was to present a simplified pushover-based procedure aimed at the development of state-dependent seismic fragility curves for multi-story moment-resisting frame structures to be used in seismic risk assessment accounting for damage accumulation. The procedure uses a semi-empirical model, which provides through Monte-Carlo simulation the joint distribution of residual displacement, normalized elongated period and strength degradation, for a given ductility demand. This information can be used to define a set of realizations of the damaged structure's pushover curve. The usefulness of this method lies in the fact that, due to the record-to-record variability of structural response to strong earthquakes, a structure subjected to a single instance of base-acceleration may fall under a generic damage state while exhibiting different realizations of basic dynamic properties, such as resistance to inertial load, stiffness and residual displacement. Such variability is typically accounted for via sequential runs to accelerogram couples that represent the alternation of two damaging shocks within an earthquake cluster, as in the case of back-to-back incremental dynamic analysis procedure.

In the simplified procedure, the first part of the sequential analysis is avoided, replaced by a simulation of the principal characteristics of the equivalent SDoF system at a given damage state. Test runs of the simplified method on plane models of ductile mid-rise moment resisting frames, showed a 90% reduction in computation cost against back-to-back IDA of a

MDoF model, or a 30% average reduction against back-to-back IDA of a surrogate SDoF system. The illustrative application presented as final part of this paper shows that the proposed methodology can represent an alternative to the more computationally intensive procedures, at least for regular structures for whom pushover-based procedures are a viable approximation.

ACKNOWLEDGEMENTS

The work present study was developed partly within the H2020-SC5-2019 *Real-time Earthquake Risk Reduction for a Resilient Europe* (RISE) project, Grant Agreement 821115, partly within the activities of the project PRIN 2017 *Assessment of Cascading Events triggered by the Interaction of Natural Hazards and Technological Scenarios involving the release of Hazardous Substances* funded by the Italian Ministry of Universities and Research, and also within the activities of the ReLUIS-DPC (Rete di Laboratori d'Ingegneria Sismica—Dipartimento di Protezione Civile) 2022−2024 research agreement, funded by the Italian Department of Civil Protection.

DATA AVAILABILITY STATEMENT

The estimated parameters needed for implementation of the predictive model in Equations (5–11) are also provided in the form of a MATHWORKS-MATLAB script, which constitutes an electronic supplement to this paper. The script is obtainable at http://wpage.unina.it/georgios.baltzopoulos/software/SDfrag.zip.

ORCID

Georgios Baltzopoulos https://orcid.org/0000-0002-0460-6558
Iunio Iervolino https://orcid.org/0000-0002-4076-2718

Notes

[1] Another very relevant motivation is that classical seismic hazard analysis only accounts for one event per cluster (i.e., the so-called mainshock).[41]

[2] The notation μ is used herein to denote both maximum transient ductility demand due to base acceleration, $|\delta_{max}|/\delta_y$, and normalized displacement response under quasi-static loading δ/δ_y, as per the typical convention in earthquake engineering literature. In all cases presented herein, the normalizing yield displacement δ_y is that of the intact structural system.

REFERENCES

1. Iervolino I, Baltzopoulos G, Chioccarelli E, Suzuki A. Seismic actions on structures in the near-source region of the 2016 central Italy sequence. *Bull Earthquake Eng*. 2017;17:5429-5447. doi:10.1007/s10518-017-0295-3
2. Sextos A, de Risi R, Pagliaroli A, et al. Local site effects and incremental damage of buildings during the 2016 Central Italy Earthquake Sequence. *Earthq Spectra*. 2018;34(4):1639-1669. doi:10.1193/100317EQS194M
3. Iervolino I, Giorgio M, Chioccarelli E. Markovian modeling of seismic damage accumulation. *Earthq Eng Struct Dyn*. 2016;45(3):441-461. doi:10.1002/eqe.2668
4. Yeo LG, Cornell AC. Building life-cycle cost analysis due to mainshock and aftershock occurrences. *Struct Saf*. 2009;31(5):396-408. doi:10.1016/j.strusafe.2009.01.002
5. Vamvatsikos D, Cornell CA. Incremental dynamic analysis. *Earthquake Eng Struct Dyn*. 2001;31(3):491-514.
6. Vamvatsikos D, Cornell CA. Applied incremental dynamic analysis. *Earthquake Spectra*. 2004;20(2):523-553. doi:10.1193/1.1737737
7. Luco N, Bazzurro P, Cornell CA. Dynamic versus static computation of the residual capacity of a mainshock-damaged building to withstand an aftershock. *13th World Conference on Earthquake Engineering*; August 1–6, 2004; Vancouver, BC, Canada.
8. Ryu H, Luco N, Uma SR, Liel AB. Developing fragilities for mainshock-damaged structures through incremental dynamic analysis. *Proceedings of the Ninth Pacific Conference on Earthquake Engineering* 2011;(225):8.
9. Goda K. Nonlinear response potential of Mainshock-Aftershock sequences from Japanese earthquakes. *Bull Seismol Soc Am*. 2012;102(5):2139-2156. doi:10.1785/0120110329
10. Ruiz-García J. Mainshock-aftershock ground motion features and their influence in building's seismic response. *J Earthquake Eng*. 2012;16(5):719-737. doi:10.1080/13632469.2012.663154
11. Goda K. Record selection for aftershock incremental dynamic analysis. *Earthq Eng Struct Dyn*. 2015;44:1157-1162. doi:10.1002/eqe
12. Baltzopoulos G, Baraschino R, Iervolino I, Vamvatsikos D. Dynamic analysis of single-degree-of-freedom systems (DYANAS): a graphical user interface for OpenSees. *Eng Struct*. 2018;177:395-408. doi:10.1016/j.engstruct.2018.09.078
13. Nazari N, van de Lindt JW, Li Y. Effect of mainshock-aftershock sequences on Woodframe building damage fragilities. *J Perform Constr Facil*. 2015;29(1). doi:10.1061/(ASCE)CF.1943-5509.0000512
14. Raghunandan M, Liel AB, Luco N. Aftershock collapse vulnerability assessment of reinforced concrete frame structures. *Earthq Eng Struct Dyn*. 2015;44(3):419-439. doi:10.1002/eqe.2478

15. Iervolino I. Assessing uncertainty in estimation of seismic response for PBEE. *Earthq Eng Struct Dyn*. 2017;46(10):1711-1723. doi:10.1002/eqe.2883
16. Baltzopoulos G, Baraschino R, Iervolino I. On the number of records for structural risk estimation in PBEE. *Earthquake Eng Struct Dyn*. 2019;48(5):489-506. doi:10.1002/eqe.3145
17. Vamvatsikos D, Cornell CA. Direct estimation of the seismic demand and capacity of MDOF systems through incremental dynamic analysis of an SDOF approximation. *J Struct Eng*. 2005;131(4):589-599. doi:10.1061/(ASCE)0733-9445(2005)131:4(589)
18. Baltzopoulos G, Baraschino R, Iervolino I, Vamvatsikos D. SPO2FRAG: software for seismic fragility assessment based on static pushover. *Bull Earthquake Eng*. 2017;15(10):4399-4425. doi:10.1007/s10518-017-0145-3
19. Luco N, Bazzurro P, Cornell CA. Dynamic versus static computation of the residual capacity of a mainshock-damaged building to withstand an aftershock. *Proceedings of the 13th World Conference on Earthquake Engineering*; Vancouver, Canada; 2004 (2405).
20. Ricci P, Manfredi V, Noto F, et al. Modeling and seismic response analysis of Italian code-conforming reinforced concrete buildings. *J Earthquake Eng*. 2018;22:105-139. doi:10.1080/13632469.2018.1527733
21. Ibarra LF, Medina RA, Krawinkler H. Hysteretic models that incorporate strength and stiffness deterioration. *Earthquake Eng Struct Dyn*. 2005;34(12):1489-1511. doi:10.1002/eqe.495
22. Lignos D, Krawinkler H. Deterioration modeling of steel components in support of collapse prediction of steel moment frames under earthquake loading. *J Struct Eng*. 2011;137(11):1291-1302. doi:10.1061/(ASCE)ST.1943-541X.0000376
23. Lignos D. Sidesway collapse of deteriorating structural systems under seismic excitations. *PhD Thesis*. 2013;53(9):1689-1699. doi:10.1017/CBO9781107415324.004
24. FEMA P440A. Effects of Strength and Stiffness Degradation on Seismic Response. Federal Emergency Management Agency; 2009.
25. Orlacchio M, Baltzopoulos G, Iervolino I. State-dependent seismic fragility via pushover analysis. 17th World Conference on Earthquake Engineering, 17WCEE Sendai, Japan—September 13th to 18th 2020; 2020.
26. Liossatou E, Fardis MN. Residual displacements of RC structures as SDOF systems. *Earthquake Eng Struct Dyn*. 2015;44(5):713-734. doi:10.1002/eqe.2483
27. Madhu Girija H, Gupta VK. Scaling of constant-ductility residual displacement spectrum. *Earthq Eng Struct Dyn*. 2020;49(3):215-233. doi:10.1002/eqe.3227
28. McKenna F. OpenSees: a framework for earthquake engineering simulation. *Comput Sci Eng*. 2011;13(4):58-66. doi:10.1109/MCSE.2011.66
29. Pacor F, Felicetta C, Lanzano G, et al. NESS v1.0: a worldwide collection of strong-motion data to investigate near source effects. *Seismol Res Lett*. 2018;89(6):2299-2313. doi:10.1785/0220180149
30. Orlacchio M, Baltzopoulos G, Iervolino I. Constant-ductility residual displacement ratios. *Proceedings of the COMPDYN2019, 7th ECCOMAS Thematic Conference on Computational Methods in Structural Dynamics and Earthquake Engineering*; Crete, Greece; June, 24–26, 2019.
31. Draper NR, Smith H. *Applied Regression Analysis*. 3rd ed. John Wiley & Sons; 1998.
32. Mardia VK. Measures of multivariate skewness and kurtosis with applications. *Biometrika*. 2019;57(3):519-530.
33. Orlacchio M. *The Effects of Seismic Sequences on Seismic Hazard and on Structural Vulnerability*. PhD Thesis (advisors: Iervolino I, Baltzopoulos G) University of Naples Federico II; 2022. http://wpage.unina.it/iuniervo/papers/Tesi_Orlacchio.pdf
34. NEHRP Consultants Joint Venture. *Evaluation of the FEMA P-695 Methodology for Quantification of Building Seismic Performance Factors (NIST GCR 10-917-8)*. 2010.
35. Franchin P, Ragni L, Rota M, Zona A. Modelling uncertainties of Italian code- conforming structures for the purpose of seismic response analysis. *J Earthquake Eng*. 2018;22(2):1964-1989. doi:10.1080/13632469.2018.1527262
36. Christopoulos C, Pampanin S. Towards performance-based design of MDOF structures with explicit consideration of residual deformations. *ISET J Earthq Technol*. 2004;41(440):53-73.
37. Baraschino R, Baltzopoulos G, Iervolino I, A note on peak inelastic displacement as a proxy for structural damage in sesmic sequences. *XIX ANIDIS Conference, Seismic Engineering in Italy*, Torino; 2022.
38. de Quevedo Iñarritu PG, Šipčić N, Bazzurro P. Engineering demand parameters for cumulative damage estimation in URM and RC buildings. In: Varum H, Benavent-Climent A, Mollaioli F, eds. *Energy-Based Seismic Engineering—IWEBSE 2023*. Springer; 2023. doi:10.1007/978-3-031-36562-1_5
39. Krawinkler H, Seneviratna GDPK. Pros and cons analysis of seismic evaluation. *Eng Struct*. 1998;20(6):452-464. doi:10.1016/S0141-0296(97)00092-8
40. Suzuki A, Iervolino I. Seismic fragility of code-conforming Italian buildings based on SDoF approximation. *J Earthquake Eng*. 2021;25(14):2873-2907. doi:10.1080/13632469.2019.1657989
41. Iervolino I, Giorgio M, Polidoro B. Sequence-based probabilistic seismic hazard analysis. *Bull Seismol Soc Am*. 2014;104(2):1006-1012. doi:10.1785/0120130207

How to cite this article: Orlacchio M, Baltzopoulos G, Iervolino I. Simplified state-dependent seismic fragility assessment. *Earthquake Engng Struct Dyn*. 2024;53:2099–2121. https://doi.org/10.1002/eqe.4105